PHYSICAL REVIEW D **94,** 034001 (2016)

LHC constraints and prospects for S_1 scalar leptoquark explaining the $\overline{B} \to D^{(*)}\tau\overline{\nu}$ anomaly

Béranger Dumont,[1] Kenji Nishiwaki,[2,*] and Ryoutaro Watanabe[1,†]

[1]*Center for Theoretical Physics of the Universe, Institute for Basic Science (IBS), Daejeon 305-811, Republic of Korea*

[2]*School of Physics, Korea Institute for Advanced Study, Seoul 02455, Republic of Korea*

(Received 1 June 2016; published 1 August 2016)

Recently, deviations in flavor observables of $\overline{B} \to D^{(*)}\tau\overline{\nu}$ have been shown between the predictions in the Standard Model and the experimental results reported by *BABAR*, Belle, and LHCb collaborations. One of the solutions to this anomaly is obtained in a class of leptoquark model with a scalar leptoquark boson S_1, which is a $SU(3)_c$ triplet and $SU(2)_L$ singlet particle with $-1/3$ hypercharge interacting with a quark-lepton pair. With well-adjusted couplings, this model can explain the anomaly and be compatible with all flavor constraints. In such a case, the S_1 boson can be pair-produced at CERN's Large Hadron Collider (LHC) and subsequently decay as $S_1^* \to t\tau$, $b\nu_\tau$, and $c\tau$. This paper explores the current 8 and 13 TeV constraints, as well as the detailed prospects at 14 TeV, of this flavor-motivated S_1 model. From the current available 8 and 13 TeV LHC searches, we obtain constraints on the S_1 boson mass for $M_{S_1} <$ 400–640 GeV depending on values of the leptoquark couplings to fermions. Then we study future prospects for this scenario at the 14 TeV LHC using detailed cut analyses and evaluate exclusion and discovery potentials for the flavor-motivated S_1 leptoquark model from searches for the $(b\nu)(\overline{b}\,\overline{\nu})$ and $(c\tau)(\overline{c}\,\overline{\tau})$ final states. In the latter case, we consider several scenarios for the identification of charm jets. As a result, we find that the S_1 leptoquark origin of the $\overline{B} \to D^{(*)}\tau\overline{\nu}$ anomaly can be probed with $M_{S_1} \lesssim 600/800$ GeV at the 14 TeV LHC with $\mathcal{L} = 300/3000$ fb^{-1} of accumulated data. One can also see that the 14 TeV LHC run II with $\mathcal{L} = 300$ fb^{-1} can exclude the S_1 leptoquark boson up to $M_{S_1} \sim 0.8$ TeV at 95% confidence level, whereas a future 14 TeV LHC with $\mathcal{L} = 3000$ fb^{-1} data has a potential to discover the S_1 leptoquark boson with its mass up to $M_{S_1} \sim 1.1$ TeV with over 5σ significance, from the $(b\nu)(\overline{b}\,\overline{\nu})$ and/or $(c\tau)(\overline{c}\,\overline{\tau})$ searches.

DOI: 10.1103/PhysRevD.94.034001

I. INTRODUCTION

An excess in the search for $\overline{B} \to D^{(*)}\tau\overline{\nu}$ reported by the *BABAR* and Belle collaborations in Refs. [1–5] has provided hints of an indirect evidence of new physics, even though the full data sample was not yet used in the Belle results [3–5]. The observables, defined as

$$R(D) \equiv \frac{\mathcal{B}(\overline{B} \to D\tau^-\overline{\nu}_\tau)}{\mathcal{B}(\overline{B} \to D\ell^-\overline{\nu}_\ell)}, \qquad R(D^*) \equiv \frac{\mathcal{B}(\overline{B} \to D^*\tau^-\overline{\nu}_\tau)}{\mathcal{B}(\overline{B} \to D^*\ell^-\overline{\nu}_\ell)}, \tag{1}$$

where $\ell = e$ or μ, are introduced for these processes in order to reduce theoretical uncertainties and separate the issue of the determination of $|V_{cb}|$ from new physics study. The standard model (SM) predicts precise values of $R(D^{(*)})$ with the help of the heavy quark effective theory [6,7]. In May 2015, the latest results from the *BABAR* [1,2], Belle [8], and LHCb [9] collaborations finally appeared all together. Consequently, we can see the significant deviations between the combined experimental results [1,2,8,9] and the SM predictions [10], which read

$$R(D)^{\rm exp} - R(D)^{\rm SM} = 0.089 \pm 0.051, \tag{2}$$

$$R(D^*)^{\rm exp} - R(D^*)^{\rm SM} = 0.070 \pm 0.022, \tag{3}$$

where the combined experimental results are privately evaluated assuming Gaussian distributions and the experimental and theoretical uncertainties are taken into account in the errors. The standard deviation with a correlation is also shown in Fig. 1, and we can see that the discrepancy reaches $\sim 4\sigma$. It is interesting that both of the deviations are "excesses" of the experimental results from the SM predictions despite negative correlations (~ -0.3) in the experiments. We put individual and combined values of the experimental results in Appendix A.

In recent years, several new physics scenarios have been investigated with respect to the excesses. In particular, as the two-Higgs-doublet model (2HDM) can give a large contribution to the tauonic B meson decays [11–15], it is studied in Refs. [16–23] to explain the large

*nishiken@kias.re.kr
†wryou1985@ibs.re.kr

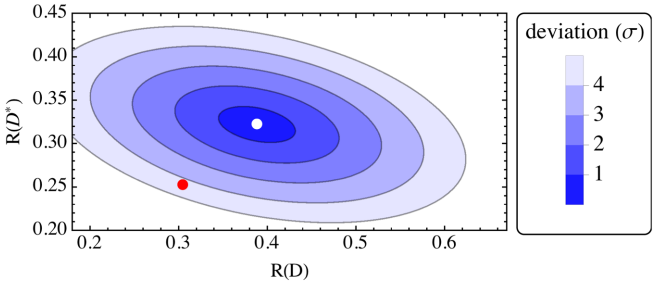

FIG. 1. Correlation between combined measurements of $R(D)$ and $R(D^*)$ [1,8,9] and comparison with the SM prediction. The red and white dots indicate the central values of the SM predictions and the combined experimental results, respectively. Both the theoretical and experimental uncertainties are taken into account when calculating the deviation contours.

deviation in $\overline{B} \to D^{(*)}\tau\overline{\nu}$. Their results imply that it is hard to accommodate the excesses in $R(D)$ and $R(D^*)$ simultaneously for the type I, II, X, and Y 2HDMs, whereas there is still allowed parameter space for the general 2HDM. The R-parity-violating minimal supersymmetric standard model is considered in Refs. [16,24–26]. It turns out that this scenario is not likely to explain the excesses and satisfy the constraint from $\overline{B} \to X_s\nu\overline{\nu}$. The extra gauge boson is also studied in the context of $\overline{B} \to D^{(*)}\tau\overline{\nu}$ in reaction to the recent update [27,28].

The other feasible and interesting scenario is given in the leptoquark model [29] on which we focus in this paper. Its potential for explaining the $\overline{B} \to D^{(*)}\tau\overline{\nu}$ anomaly is studied in Refs. [10,16,30,31]. As a consequence of the recent study in Ref. [10], three types of the leptoquark bosons can explain the excess without any inconsistency with the constraint from $\overline{B} \to X_s\nu\overline{\nu}$. By limiting the flavor structure of leptoquark couplings, correlations to other processes, especially to the R_K anomaly, are also discussed in Refs. [27,32–36]. Note that scalar leptoquarks are also useful for explaining the $h \to \mu\tau$ anomaly in CMS (and ATLAS) [34,37–39].

To explain the central combined experimental values of $R(D^{(*)})$ in any case, somewhat large couplings of the leptoquark boson to the third- (and second-, in part) generation quarks and leptons are required. Hence, the leptoquark search for the third generation at the Large Hadron Collider (LHC) can be significant. Since the color $SU(3)$ charge is assigned, the leptoquark bosons are dominantly pair-produced at the hadron collider and its cross section is independent of the couplings to fermions. Thus, the direct search of the leptoquark boson gives a constraint on a branching ratio of its decay into fermions. In this paper, we study the leptoquark search at the LHC, including the second- and third-generation quarks and leptons in the final state, where it is motivated by the flavor anomaly in $\overline{B} \to D^{(*)}\tau\overline{\nu}$.

This paper is organized as follows. At first, after briefly reviewing the leptoquark model, we show the current status of explaining the $\overline{B} \to D^{(*)}\tau\overline{\nu}$ anomaly and constraints from a related flavor process in the model in Sec. II. Then, we summarize present collider studies at the LHC and apply them to the model in Sec. III. In Sec. IV, we provide detailed analysis cuts, which are performed for 14 TeV LHC searches. In turn, we show our results and discuss future prospects for exclusion and discovery potentials of the leptoquark boson in Sec. V. Finally, a summary is provided in Sec. VI.

II. LEPTOQUARK MODEL AND FLAVOR OBSERVABLES

Here, we give a brief review on the possible types of leptoquarks and their interactions. Then we summarize the contribution to the process in $b \to c\tau\overline{\nu}$, which leads to $\overline{B} \to D^{(*)}\tau\overline{\nu}$ at the hadron level, for all possible cases.

A. Classification

Some of the new physics scenarios, especially for grand unifications of the fundamental interactions, contain new scalar and vector bosons which interact with quarks and leptons. This kind of boson is called a leptoquark and carries both the baryon and lepton numbers together with color and electric charges. It is known [29] that there are ten types of leptoquarks with the general dimensionless $SU(3)_c \times SU(2)_L \times U(1)_Y$ invariant and flavor nondiagonal couplings.[1] Among them, six leptoquark (LQ) bosons are relevant for the process $b \to c\ell\overline{\nu}$. The Lagrangian for the term interacting with SM fermions is given by

$$\mathcal{L}^{\mathrm{LQ}} = \mathcal{L}^{\mathrm{LQ}}_{F=0} + \mathcal{L}^{\mathrm{LQ}}_{F=-2}, \tag{4}$$

$$\mathcal{L}^{\mathrm{LQ}}_{F=0} = (h^{ij}_{1L}\overline{Q}^i_L\gamma_\mu L^j_L + h^{ij}_{1R}\overline{d}^i_R\gamma_\mu \ell^j_R)U^\mu_1 + h^{ij}_{3L}\overline{Q}^i_L\boldsymbol{\sigma}\gamma_\mu L^j_L\boldsymbol{U}^\mu_3 + (h^{ij}_{2L}\overline{u}^i_R L^j_L + h^{ij}_{2R}\overline{Q}^i_L i\sigma_2\ell^j_R)R_2 + \mathrm{H.c.}, \tag{5}$$

$$\mathcal{L}^{\mathrm{LQ}}_{F=-2} = (g^{ij}_{1L}\overline{Q}^{c,j}_L i\sigma_2 L^j_L + g^{ij}_{1R}\overline{u}^{c,i}_R\ell^j_R)S_1 + g^{ij}_{3L}\overline{Q}^{c,i}_L i\sigma_2\boldsymbol{\sigma}L^j_L\boldsymbol{S}_3 + (g^{ij}_{2L}\overline{d}^{c,i}_R\gamma_\mu L^j_L + g^{ij}_{2R}\overline{Q}^{c,i}_L\gamma_\mu\ell^j_R)V^\mu_2 + \mathrm{H.c.}, \tag{6}$$

where h^{ij} and g^{ij} are the dimensionless couplings; S_1, $\boldsymbol{S}_3$, and R_2 are scalar leptoquark bosons; U^μ_1, $\boldsymbol{U}^\mu_3$, and V^μ_2 are vector leptoquark bosons; index i (j) indicates the generation of quarks (leptons); and $\psi^c = C\overline{\psi}^T = C\gamma^0\psi^*$ is the charge-conjugated fermion field of ψ. These six leptoquark bosons (S_1, $\boldsymbol{S}_3$, R_2, U_1, $\boldsymbol{U}_3$, and V_2) can

[1] In this paper, we do not consider possible "diquark" interactions even though they are allowed by the SM gauge invariance in general. As is widely known, if leptoquark and diquark interactions coexist, both the baryon and lepton numbers are violated so that the proton becomes unstable. Note that among the three scalar leptoquarks shown in Table I, R_2 can avoid such an unstable proton (within renormalizable interactions) since no renormalizable diquark interaction is written down [40].

TABLE I. Quantum numbers of scalar and vector leptoquarks.

	Spin	$F = 3B + L$	$SU(3)_c$	$SU(2)_L$	$U(1)_{Y=Q-T_3}$
S_1	0	−2	3^*	1	1/3
$\boldsymbol{S}_3$	0	−2	3^*	3	1/3
R_2	0	0	3	2	7/6
V_2	1	−2	3^*	2	5/6
U_1	1	0	3	1	2/3
$\boldsymbol{U}_3$	1	0	3	3	2/3

contribute to $\overline{B} \to D^{(*)}\tau\overline{\nu}$. In Table I, we summarize the quantum numbers of the leptoquark bosons. Here we define the fermions in the gauge eigenbasis and follow the treatment in Ref. [10] such that Yukawa couplings of the up-type quarks and the charged leptons are diagonal, while the down-type quark fields are rotated into the mass eigenstate basis by the Cabibbo-Kobayashi-Maskawa (CKM) matrix.

B. Contribution to $\overline{B} \to D^{(*)}\tau\overline{\nu}$

The leptoquark bosons which have interactions in Eqs. (4)–(6) can contribute to $\overline{B} \to D^{(*)}\tau\overline{\nu}$ at the tree level. The effective Lagrangian for $b \to c\tau\overline{\nu}_l$ is written [10] as

$$-\mathcal{L}_{\rm eff} = (C_{\rm SM}\delta_{l\tau} + C^l_{\mathcal{V}_1})\mathcal{O}^l_{\mathcal{V}_1} + C^l_{\mathcal{V}_2}\mathcal{O}^l_{\mathcal{V}_2} + C^l_{\mathcal{S}_1}\mathcal{O}^l_{\mathcal{S}_1} + C^l_{\mathcal{S}_2}\mathcal{O}^l_{\mathcal{S}_2} + C^l_{\mathcal{T}}\mathcal{O}^l_{\mathcal{T}}, \quad (7)$$

where the effective operators are defined as

$$\mathcal{O}^l_{\mathcal{V}_1} = (\overline{c}_L\gamma^\mu b_L)(\overline{\tau}_L\gamma_\mu\nu_{lL}), \quad (8)$$

$$\mathcal{O}^l_{\mathcal{V}_2} = (\overline{c}_R\gamma^\mu b_R)(\overline{\tau}_L\gamma_\mu\nu_{lL}), \quad (9)$$

$$\mathcal{O}^l_{\mathcal{S}_1} = (\overline{c}_L b_R)(\overline{\tau}_R\nu_{lL}), \quad (10)$$

$$\mathcal{O}^l_{\mathcal{S}_2} = (\overline{c}_R b_L)(\overline{\tau}_R\nu_{lL}), \quad (11)$$

$$\mathcal{O}^l_{\mathcal{T}} = (\overline{c}_R\sigma^{\mu\nu} b_L)(\overline{\tau}_R\sigma_{\mu\nu}\nu_{lL}), \quad (12)$$

and the Wilson coefficients in the leptoquark model are given by

$$C_{\rm SM} = 2\sqrt{2}G_F V_{cb}, \quad (13)$$

$$C^l_{\mathcal{V}_1} = \sum_{k=1}^{3} V_{k3}\left[\frac{g^{kl}_{1L}g^{23*}_{1L}}{2M^2_{S_1}} - \frac{g^{kl}_{3L}g^{23*}_{3L}}{2M^2_{S_3}} + \frac{h^{2l}_{1L}h^{k3*}_{1L}}{M^2_{U_1}} - \frac{h^{2l}_{3L}h^{k3*}_{3L}}{M^2_{U_3}}\right], \quad (14)$$

$$C^l_{\mathcal{V}_2} = 0, \quad (15)$$

$$C^l_{\mathcal{S}_1} = \sum_{k=1}^{3} V_{k3}\left[-\frac{2g^{kl}_{2L}g^{23*}_{2R}}{M^2_{V_2}} - \frac{2h^{2l}_{1L}h^{k3*}_{1R}}{M^2_{U_1}}\right], \quad (16)$$

$$C^l_{\mathcal{S}_2} = \sum_{k=1}^{3} V_{k3}\left[-\frac{g^{kl}_{1L}g^{23*}_{1R}}{2M^2_{S_1}} - \frac{h^{2l}_{2L}h^{k3*}_{2R}}{2M^2_{R_2}}\right], \quad (17)$$

$$C^l_{\mathcal{T}} = \sum_{k=1}^{3} V_{k3}\left[\frac{g^{kl}_{1L}g^{23*}_{1R}}{8M^2_{S_1}} - \frac{h^{2l}_{2L}h^{k3*}_{2R}}{8M^2_{R_2}}\right], \quad (18)$$

at the energy scale $\mu = M_X$, where X represents a leptoquark. The SM contribution is given by $C_{\rm SM}$. The index l denotes the generation of the neutrino which, in general, needs not be the third one in this case. The CKM matrix element is denoted as $V_{ij} \equiv V_{u_i d_j}$. We note that we take the correct mass eigenstate basis for the fermions and, thus, the CKM matrix elements appear in the Wilson coefficients.

As can be seen in Eqs. (14)–(18), several leptoquark bosons with several combinations of the couplings can contribute to $b \to c\tau\overline{\nu}_l$. Those contributions can be classified as

(i) $C^l_{\mathcal{S}_2} = -4C^l_{\mathcal{T}}$ mediated by S_1 boson with nonzero value of $(g_{1L}g^*_{1R})$,
(ii) $C^l_{\mathcal{S}_2} = 4C^l_{\mathcal{T}}$ by R_2 boson with $(h_{2L}h^*_{2R})$,
(iii) $C^l_{\mathcal{V}_1}$ by S_1, $\boldsymbol{S}_3$, U_1, or $\boldsymbol{U}_3$ bosons with $(g_{1L}g^*_{1L})$, $(g_{3L}g^*_{3L})$, $(h_{1L}h^*_{1L})$, or $(h_{3L}h^*_{3L})$,
(iv) $C^l_{\mathcal{S}_1}$ by U_1 or V_2 bosons with $(h_{1L}h^*_{1R})$ or $(g_{2L}g^*_{2R})$.

It is interesting that the tensor-type operator appears in the S_1- and R_2-type leptoquark models [41]. To evaluate those effects on the observables $R(D)$ and $R(D^*)$, the running effect of $C^l_Y(\mu)$ (Y showing types of the effective operators) from $\mu = M_X$ to $\mu = \mu_b$, where μ_b is the mass scale of the bottom quark, must be taken into account. Due to the fact that the vector and axial-vector currents are not renormalized and their anomalous dimensions vanish, $\mathcal{V}_{1,2}$ do not receive the running effect. On the other hand, a scale dependence in the scalar $\mathcal{S}_{1,2}$ and tensor $\mathcal{T}$ currents exists and is approximately evaluated as

$$C_{\mathcal{S}_{1,2}}(\mu_b) = \left[\frac{\alpha_s(m_t)}{\alpha_s(\mu_b)}\right]^{-\frac{12}{23}}\left[\frac{\alpha_s(m_{\rm LQ})}{\alpha_s(m_t)}\right]^{-\frac{4}{7}} C_{\mathcal{S}_{1,2}}(m_{\rm LQ}), \quad (19)$$

$$C_{\mathcal{T}}(\mu_b) = \left[\frac{\alpha_s(m_t)}{\alpha_s(\mu_b)}\right]^{\frac{4}{23}}\left[\frac{\alpha_s(m_{\rm LQ})}{\alpha_s(m_t)}\right]^{\frac{4}{21}} C_{\mathcal{T}}(m_{\rm LQ}), \quad (20)$$

where $\alpha_s(\mu)$ is a running QCD coupling at a scale μ. In the following study, we take $\mu_b = 4.2$ GeV, and the flavor observables are evaluated at this scale.

The branching ratios of $\overline{B} \to D^{(*)}\tau\overline{\nu}$ can be calculated, given hadronic form factors that are precisely estimated with the use of the heavy quark effective theory. The formulas in terms of the helicity amplitudes are found, e.g., in Refs. [10,16].

TABLE II. Allowed ranges for the products of leptoquark couplings assuming nonzero value in only one specific product of the couplings and zero in the others, at the leptoquark mass 1 TeV. The values are 2σ boundaries of the allowed region for the $\bar{B} \to D^{(*)}\tau\bar{\nu}$ case. The constraints from $\bar{B} \to X_s\nu\bar{\nu}$ are presented at 90% C.L. which can be applied for each possible combination of fermion generation (i, j). Here, we assume that the product of the couplings is real or purely imaginary. When the value can be real and purely imaginary, we show only the real case.

Leptoquark	$\bar{B} \to D^{(*)}\tau\bar{\nu}$ $(i = 1, 2)$	$\bar{B} \to X_s\nu\bar{\nu}$
S_1	$-0.87 < g_{1L}^{33} g_{1R}^{23*} < -0.54$, $1.64 < \lvert g_{1L}^{3i} g_{1R}^{23*}\rvert < 1.81$, $0.19 < g_{1L}^{33} g_{1L}^{23*} < 0.48$, $-5.59 < g_{1L}^{33} g_{1L}^{23*} < -5.87$, $1.04 < \lvert g_{1L}^{3i} g_{1L}^{23*}\rvert < 1.67$	$\lvert g_{1L}^{3i} g_{1L}^{2j*}\rvert \lesssim 0.15$
$\boldsymbol{S}_3$	$0.19 < g_{3L}^{33} g_{3L}^{23*} < 0.48$, $-5.59 < g_{3L}^{33} g_{3L}^{23*} < -5.87$, $1.04 < \lvert g_{3L}^{3i} g_{3L}^{23*}\rvert < 1.67$	$\lvert g_{3L}^{3i} g_{3L}^{2j*}\rvert \lesssim 0.15$
R_2	$1.64 < \lvert \mathrm{Im}(h_{2L}^{2i} h_{2R}^{33*})\rvert < 1.81$	$\cdots$
V_2	$g_{2L}^{3i} g_{2R}^{23*}$: no region within 2σ	$\lvert g_{2L}^{3i} g_{2L}^{2j*}\rvert \lesssim 0.07$
U_1	$0.10 < h_{1L}^{23} h_{1L}^{33*} < 0.24$, $-2.94 < h_{1L}^{23} h_{1L}^{33*} < -2.80$, $0.52 < \lvert h_{1L}^{2i} h_{1L}^{33*}\rvert < 0.84$, $h_{1L}^{2i} h_{1R}^{33*}$: no region within 2σ	$\cdots$
$\boldsymbol{U}_3$	$0.10 < h_{3L}^{23} h_{3L}^{33*} < 0.24$, $-2.94 < h_{3L}^{23} h_{3L}^{33*} < -2.80$, $0.52 < \lvert h_{3L}^{2i} h_{3L}^{33*}\rvert < 0.84$	$\lvert h_{3L}^{2i} h_{3L}^{3j*}\rvert \lesssim 0.04$

C. Present bound from $\overline{B} \to D^{(*)}\tau\bar{\nu}$ and $\overline{B} \to X_s\nu\bar{\nu}$

In Ref. [10], a precise study has been done for the present constraints on the leptoquark bosons from $\overline{B} \to D^{(*)}\tau\bar{\nu}$ together with $\overline{B} \to X_s\nu\bar{\nu}$, which is also affected by S_1, $\boldsymbol{S}_3$, V_2, and $\boldsymbol{U}_3$ leptoquark bosons [42] with partly same combinations of the couplings [10]. The experimental upper limit on the inclusive branching ratio of $\overline{B} \to X_s\nu\bar{\nu}$ is given as

$$\mathcal{B}(\overline{B} \to X_s\nu\bar{\nu}) < 6.4 \times 10^{-4}, \tag{21}$$

at the 90% confidence level (C.L.) by the ALEPH Collaboration [43]. As an illustration for the bound from $\overline{B} \to D^{(*)}\tau\bar{\nu}$ and $\overline{B} \to X_s\nu\bar{\nu}$, we show the allowed range of the product of the couplings in Table II. In this table, we assume that only one specific combination of the product, having a real or purely imaginary value,[2] and one type of leptoquark bosons exist with its mass to be 1 TeV. We also neglect the couplings with $k \neq 3$ due to double Cabibbo suppressions. Namely, we keep only the leading terms proportional to $V_{33} = V_{tb}$ in Eqs. (14)–(18). We can see that the $\boldsymbol{S}_3$ and $\boldsymbol{U}_3$ leptoquarks cannot satisfy both constraints from $\overline{B} \to D^{(*)}\tau\bar{\nu}$ and $\overline{B} \to X_s\nu\bar{\nu}$ at the same time. The V_2 leptoquark has no way to explain the anomaly in $\overline{B} \to D^{(*)}\tau\bar{\nu}$. As for the R_2 and U_1 leptoquarks, the condition from $\overline{B} \to D^{(*)}\tau\bar{\nu}$ is fulfilled, whereas no constraint comes from $\overline{B} \to X_s\nu\bar{\nu}$.

A further more interesting result is obtained in the S_1 leptoquark case as follows. The allowed region for $g_{1L}^{3i} g_{1L}^{23*}$ from $\overline{B} \to D^{(*)}\tau\bar{\nu}$ is inconsistent with that for $\lvert g_{1L}^{3i} g_{1L}^{2j*}\rvert$ from $\overline{B} \to X_s\nu\bar{\nu}$. On the other hand, the S_1 leptoquark boson can satisfy both of the constraints, in the case that g_{1L}^{2j} is sufficiently small and the product $g_{1L}^{3i} g_{1R}^{23*}$ has $O(1)$ magnitude (for $M_{S_1} = O(1)$ TeV). In particular, when $g_{1L}^{3i} g_{1R}^{23*}$ is real, the best-fit value to explain the anomaly is given as

$$\frac{g_{1L}^{3i} g_{1R}^{23*}}{2M_{S_1}^2} \simeq \begin{cases} -0.26 C_{\mathrm{SM}} & \text{for } i = 3 \\ \pm 0.64 C_{\mathrm{SM}} & \text{for } i \neq 3 \ (i = 1 \text{ or } 2) \end{cases}, \tag{22}$$

where C_{SM} is defined in Eq. (13) and the other couplings are assumed to be zero. This means that 26% of the SM contribution is required for the case of $i = 3$. In the case of $i = 1$ or 2, the sign of the right-hand side of Eq. (22) is not determined. Also, this sign does not affect the physics discussed in this paper since no interference term appears in the decay sequence of S_1 in the collider. Such a large effect, motivated by the flavor anomaly, can be significant at the collider search and, thus, will be studied below. In the following, we focus on the S_1 leptoquark boson and study the collider phenomenology at the LHC while keeping the condition to explain the anomaly in $\overline{B} \to D^{(*)}\tau\bar{\nu}$.

III. COLLIDER STUDY

In general, the leptoquark model contains a lot of interaction terms to quarks and leptons and thus there are many possible signals for a collider search. Given the condition in Eq. (22) motivated by the anomaly in $\overline{B} \to D^{(*)}\tau\bar{\nu}$, the minimal setup is

$$g_{1L}^{3i} \neq 0, \qquad g_{1R}^{23} \neq 0, \qquad \text{others} = 0, \tag{23}$$

namely, nonzero couplings only in the terms $\overline{Q}_L^{c,3} i\sigma_2 L_L^i S_1$ and $\overline{e}_R^c \tau_R S_1$ (and their Hermitian conjugates). In our study, we obey this setup and, thus, consider the phenomenology for the decays $S_1^* \to t\ell$, $b\nu_\ell$ and $c\tau$ at the LHC. As is the case in the previous section, we ignore the doubly Cabibbo-suppressed terms from the CKM matrix elements and consider only the $V_{33} = V_{tb}$ terms of Eqs. (17) and (18) in the following paper.

[2]When the product of the couplings can be real and purely imaginary, we show only the real case.

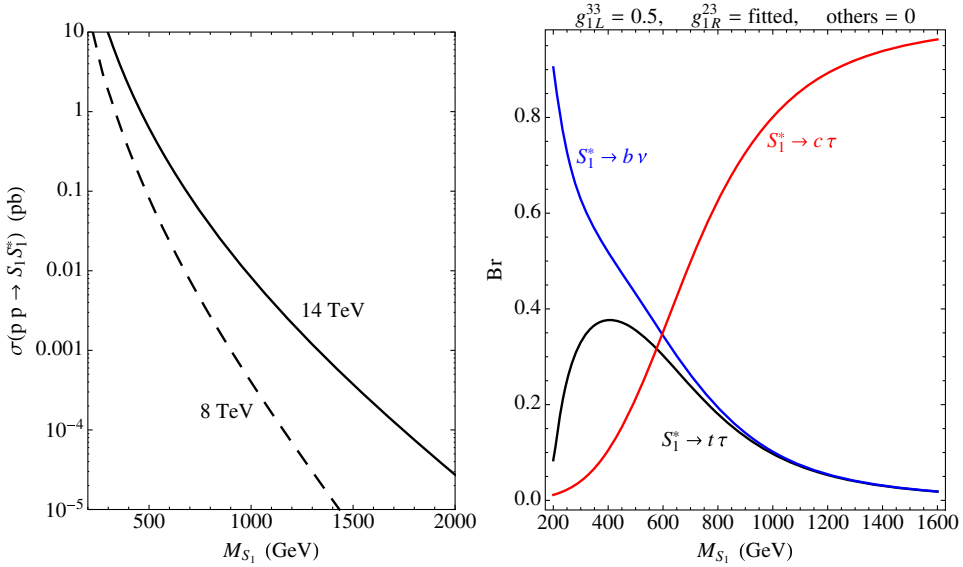

FIG. 2. Pair production cross sections (left) and decay branching ratios (right) of the S_1 leptoquark boson as a function of its mass. The NLO cross sections at 8 and 14 TeV are shown as indicated by the legend in the left figure. The branching ratios for $S_1^* \to t\tau$, $S_1^* \to b\nu_\tau$, and $S_1^* \to c\tau$ are denoted by black, blue, and red curves in the right figure, respectively. We take $g_{1L}^{33} = 0.5$ and g_{1R}^{23} is fixed by following Eq. (22) so as to explain $R(D)$ and $R(D^*)$ simultaneously.

A. Production process

Since a leptoquark boson has $SU(3)$ color charge, it is expected that a pair production of leptoquark bosons by the QCD interaction is significant. We note that the QCD pair production does not depend on the couplings defined in Eqs. (4)–(6). In this paper, we investigate the pair-produced leptoquark bosons by QCD at the LHC.[3]

Thus, our target signal at the LHC is produced through $pp \to S_1 S_1^*$, where p indicates a proton. The production cross section in the leptoquark model has been evaluated at the next-to-leading order (NLO) [47–49]. With the use of PROSPINO2.1 [47,50], we show the plot for $\sigma(pp \to S_1 S_1^*)$ as a function of M_{S_1} at $\sqrt{s} = 8$ and 14 TeV in Fig. 2.

B. Decay process

In the minimal setup for our study, the possible decay processes are $S_1^* \to t\ell^i$, $b\nu_{\ell^i}$ for $g_{1L}^{3i} \neq 0$ and $S_1^* \to c\tau$ for $g_{1R}^{23} \neq 0$, where we define $\ell^1 = e$, $\ell^2 = \mu$, and $\ell^3 = \tau$. To see the feature, we show the branching ratios for these three decay modes for $g_{1L}^{33} = 0.5$ in Fig. 2 as an example. Here, the coupling g_{1R}^{23} is automatically fixed as the relation in Eq. (22), namely, $g_{1R}^{23} = -0.52 C_{\rm SM} M_{S_1}^2 / g_{1L}^{33}$. The decay branch $S_1^* \to c\tau$ becomes the dominant one for S_1 with a large mass.

Therefore, there are six final states of the signal event from the pair production for each lepton generation ℓ^i. The final states can be categorized into two parts (here we omit the particle/antiparticle assignment):

(i) independent of the flavor of ℓ: $(b\nu_\ell)(b\nu_\ell)$, $(c\tau)(c\tau)$, $(b\nu_\ell)(c\tau)$.
(ii) dependent on the flavor of ℓ: $(t\ell)(t\ell)$, $(t\ell)(b\nu_\ell)$, $(t\ell)(c\tau)$.

The final states in the former category are independent of the choice of ℓ, and thus can be analyzed without specifying ℓ. As for the latter category, on the other hand, it is required to investigate every lepton flavor due to differences in the efficiency, acceptance, and tagging methods.

C. Current status

1. $(b\nu_\ell)(\bar{b}\bar{\nu}_\ell)$ and $(t\tau)(\bar{t}\bar{\tau})$

Up to the present, there exist two CMS and ATLAS searches which can be applied to the final states of $(b\nu_\ell)(\bar{b}\bar{\nu}_\ell)$ for the LHC run I. In Refs. [51,52], the ATLAS and CMS collaborations have searched for the third-generation squarks and obtained exclusion limits in terms of the lightest bottom squark ($\tilde{b}_1$) and lightest neutralino ($\tilde{\chi}_1^0$) masses, where the final state is $(b\tilde{\chi}_1^0)(\bar{b}\tilde{\chi}_1^0)$ with zero or more jets. Results obtained for $M_{\tilde{\chi}_1^0} = 0$ can be directly translated into results for $(b\nu_\ell)(\bar{b}\bar{\nu}_\ell)$ in the scalar leptoquark model. The CMS analysis in Ref. [52] gives the

[3]A t-channel exchange of a lepton can also produce a pair of leptoquark bosons by the couplings in Eqs. (4)–(6). This contribution is, however, much suppressed unless the couplings are very large such as $g_{1L}^{11} \sim 2$, e.g., see Ref. [44]. When the leptoquark couplings are much larger, single production in association with a lepton becomes important as well [45,46]. On the other hand, in our configuration, only the charm, bottom, and top quarks appear through the leptoquark interactions, which are highly parton-distribution-function (PDF) suppressed or do not exist as a parton when $\sqrt{s} = 8$ or 14 TeV. Thereby, only the QCD pair production is relevant in our setup even when the couplings are $g_{1L}^{3i}, g_{1R}^{23} \sim 2$.

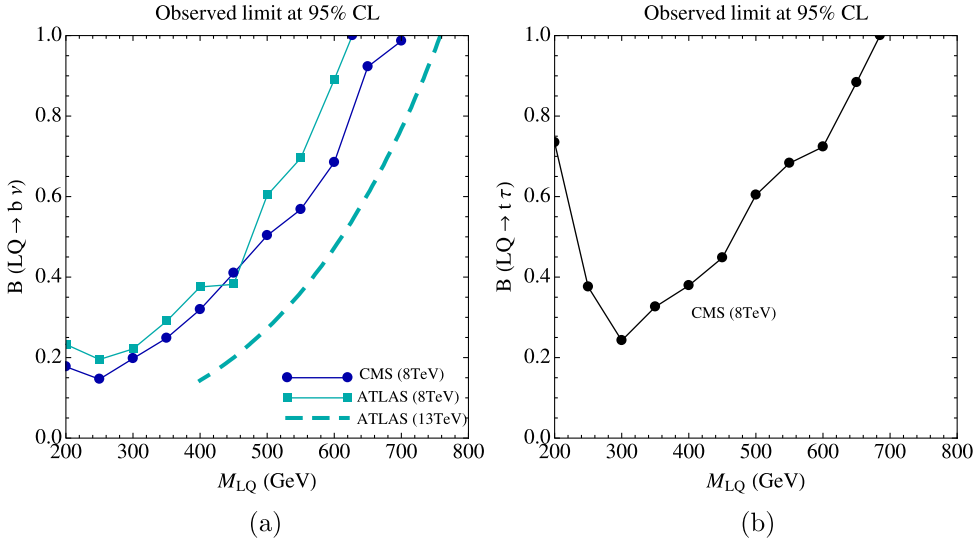

FIG. 3. Observed upper limits on the branching ratio at 95% C.L. for (a) LQ → $b\nu_\ell$ from the CMS (blue) and ATLAS (cyan) analyses, and (b) LQ → $t\tau$ obtained from the CMS analysis.

observed limit on the branching ratio for LQ → $b\nu_\ell$. On the other hand, a direct bound on third-generation leptoquarks through the $(b\nu_\ell)(\bar{b}\bar{\nu}_\ell)$ channel was provided by ATLAS [53]. In addition, results of the bottom squark search at the 13 TeV LHC have been recently reported by the ATLAS Collaboration [54]. However, since this report lacks information for the observed limit on the cross section, we only obtain a rough bound for the leptoquark case as shown below. In Ref. [55], the CMS Collaboration has also analyzed the pair production of third-generation scalar leptoquarks decaying into $(t\tau)(\bar{t}\,\bar{\tau})$.

In Fig. 3, we show the exclusion plot for $\mathcal{B}(\mathrm{LQ} \to b\nu_\ell)$ and $\mathcal{B}(\mathrm{LQ} \to t\tau)$ as a function of the LQ mass, where LQ indicates an arbitrary scalar leptoquark boson. The result from the ATLAS search is translated from the one in Ref. [51], by taking into account the NLO cross section of LQ pair production [49] and by assuming the narrow width approximation for the total decay width of LQ. We confirmed that our interpretation from the ATLAS bottom squark search is close to the ATLAS official bound in Ref. [51]. Note that the 13 TeV recast shown in the figure is estimated by obtaining the observed limit on the cross section as $\sigma(pp \to \tilde{b}_1\tilde{b}_1) \simeq 22.8$ fb at the 95% C.L. exclusion point [54] and then applying it to the leptoquark case. In this rough estimation, the mass dependence on the observed limit is neglected since such information is not available in this report. Hence, this estimation should not be applied to the small LQ mass region less than around 400 GeV because the acceptance times efficiency can be drastically changed in this region.

2. $(c\tau)(\bar{c}\,\bar{\tau})$

There is a CMS search for the pair-produced scalar leptoquarks decaying to $(b\tau)(\bar{b}\,\bar{\tau})$ [56]. It is possible to reinterpret this result to put a constraint on the leptoquark boson decays into $(c\tau)(\bar{c}\,\bar{\tau})$, since c jets are close cousins of b jets, and the b-tagging algorithms actually have a reasonably high probability of tagging a c jet as a b jet (mistagging).[4] For this, however, it is necessary to quantify the probability of misidentifying c jets as being b jets.

In this analysis, jets are b-tagged using the combined secondary vertex (CSV) algorithm with the loose operating point (CSVL). Furthermore, only one jet is required to be b-tagged, while the second one is selected whether or not it is b-tagged. The latest preliminary note on b-tagging at $\sqrt{s} = 8$ TeV is obtained in Ref. [60] but does not contain the information we need. However, tagging and mistagging efficiencies for the CSVL can be found in the $\sqrt{s} = 7$ TeV b-tagging paper [61]. There, we find

$$\varepsilon_{\mathrm{CSVL}}^{b\,\mathrm{jet}} = 85\%, \qquad \varepsilon_{\mathrm{CSVL}}^{c\,\mathrm{jet}} = 45\%. \tag{24}$$

The CMS analysis has two relevant signal regions, $e\tau_\mathrm{h}$ and $\mu\tau_\mathrm{h}$, targeting final states with two τ leptons, one decaying hadronically and the other leptonically. In each of these two signal regions, the number of expected events per integrated luminosity $\mathcal{L}$ for a scalar LQ boson decaying into $c\tau$ is given by

$$\begin{aligned} n_{\mathrm{LQ}\to c\tau}/\mathcal{L} &= \sigma_{pp\to \mathrm{LQLQ}^*} \times (A\times\varepsilon)_{\mathrm{LQ}\to b\tau} \frac{\varepsilon_{\mathrm{CSVL}}^{c\,\mathrm{jet}}}{\varepsilon_{\mathrm{CSVL}}^{b\,\mathrm{jet}}} \\ &\approx 0.53\sigma_{pp\to \mathrm{LQLQ}^*}(A\times\varepsilon)_{\mathrm{LQ}\to b\tau}, \end{aligned} \tag{25}$$

[4]Note that similar discussions are found in how to measure the charm Yukawa coupling to the Higgs boson in Refs. [57–59].

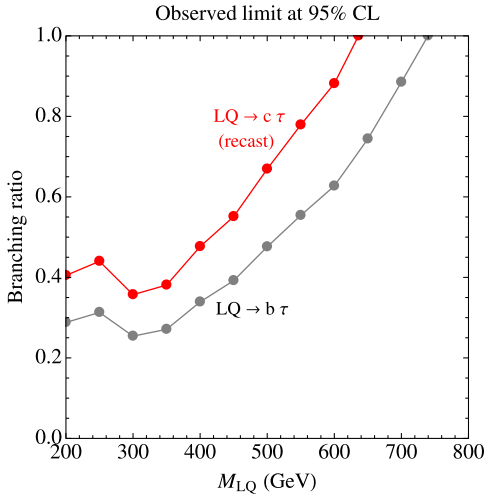

FIG. 4. Observed upper limits on the branching ratio at 95% C.L. for LQ → $b\tau$ (gray) and LQ → $c\tau$ (red) as a function of the leptoquark mass.

where $(A \times \varepsilon)_{LQ \to b\tau}$ is the acceptance times efficiency of the selection criteria. As the nature of the jet has very little influence on the acceptance times efficiency, apart from the tagging requirement, the factor $\varepsilon^{c\,\mathrm{jet}}_{\mathrm{CSVL}}/\varepsilon^{b\,\mathrm{jet}}_{\mathrm{CSVL}}$ can be considered as a rescaling factor for the cross section. Therefore, it is straightforward to recast the results in Ref. [56] for $(c\tau)(\bar{c}\,\bar{\tau})$. In Fig. 4, we show the exclusion plot for $\mathcal{B}(\mathrm{LQ} \to b\tau)$ and $\mathcal{B}(\mathrm{LQ} \to c\tau)$.

3. Constraint on S_1 leptoquark model

We can apply the present limits on the branching ratios shown above to the specific model. For the S_1 leptoquark with the minimal setup of Eq. (23), the branching ratios for $S_1^* \to t\ell^i$, $b\nu_{\ell^i}$, and $c\tau$ are controlled by g^{3i}_{1L}, g^{23}_{1R}, and M_{S_1}. If we take $g^{3i}_{1L} = 0$ for $i = 1, 2$ and keep the condition in Eq. (22), two of g^{33}_{1L}, g^{23}_{1R}, and M_{S_1} remain free parameters. The excluded region in the (M_{S_1}, g^{33}_{1L}) plane for this case is given in Fig. 5, where the coupling g^{23}_{1R} is fixed as $g^{23}_{1R} = -0.52 C_{\mathrm{SM}} M^2_{S_1}/g^{33}_{1L}$. The colored regions are excluded from the corresponding searches at ATLAS or CMS as denoted in the figure. We can see that $M_{S_1} < 530$ GeV and $M_{S_1} < 640$ GeV are ruled out for $g^{33}_{1L} \gtrsim 0.5$ and $g^{33}_{1L} \lesssim 0.2$, respectively, from the 8 TeV LHC searches. The rough estimate for $S_1^* \to b\nu_{\ell^i}$ from the 13 TeV analysis is also shown with the dashed line. In this setup, for a small g^{33}_{1L} and a large M_{S_1}, the coupling g^{23}_{1R} and the total decay width Γ_{S_1} can be large. Thus, we show the regions for $g^{23}_{1R} > 4\pi$ and $\Gamma_{S_1}/M_{S_1} > 0.2$ with dark yellow and black colors, respectively. The right panel in Fig. 5 shows the exclusion in the (M_{S_1}, g^{3i}_{1L}) plane for $i = 1$ or 2 with the condition $g^{23}_{1R} = -1.28 C_{\mathrm{SM}} M^2_{S_1}/g^{3i}_{1L}$, assuming the other couplings to be zero. In this case, the search for $S_1^* \to t\tau$ is irrelevant. To conclude, the white regions in the figure are totally allowed by both the 8 TeV LHC searches and the flavor observables in $\bar{B} \to D^{(*)}\tau\bar{\nu}$ and $\bar{B} \to X_s \nu\bar{\nu}$.

IV. ANALYSIS AT 14 TEV LHC

Recently, the LHC run II successfully started at an energy of 13 TeV. The updated LHC experiments at 13 and 14 TeV will greatly improve the discovery potential for the leptoquark models as well as many other new physics candidates. In this section, we provide the detailed

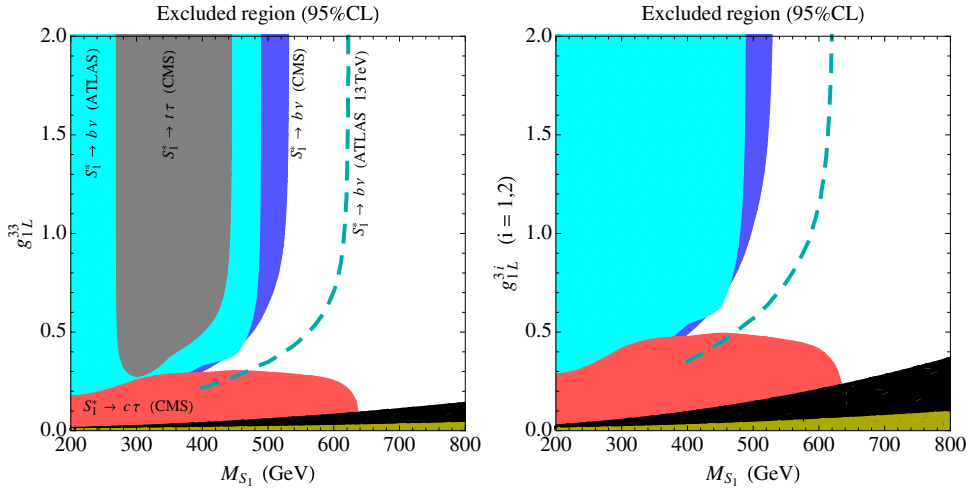

FIG. 5. (left) An excluded region plot in the (M_{S_1}, g^{33}_{1L}) plane for the S_1 leptoquark model, obtained by assuming that $g^{23}_{1R} = -0.52 C_{\mathrm{SM}} M^2_{S_1}/g^{33}_{1L}$ and the other couplings are zero; (right) a plot in the (M_{S_1}, g^{3i}_{1L}) plane for $i = 1$ or 2 by assuming that $g^{23}_{1R} = -1.28 C_{\mathrm{SM}} M^2_{S_1}/g^{3i}_{1L}$ and others are zero. Each colored region is excluded from the ATLAS or CMS analyses for the decay modes as exhibited in the legend. In the black region, the ratio of the width to mass of S_1 boson becomes larger than 0.2, where the narrow width approximation does not work correctly. The dark yellow color shows the region for $g^{23}_{1R} > 4\pi$.

procedure of our analyses to obtain our numerical results at the 14 TeV LHC. Based on the analyses given in this section, prospects and results by simulations for our leptoquark model are shown in the next section. Our target signals for the analyses are $(b\nu_\ell)(\bar{b}\bar{\nu}_\ell)$ and $(c\tau)(\bar{c}\,\bar{\tau})$ from the $S_1^{(*)}$ pair production. Signal and background events are simulated in the cluster system provided at CTPU-IBS.

A. $S_1^* \to b\nu$

As already mentioned in the previous section, the event topology of the final state from $pp \to S_1^* S_1 \to (b\nu_\ell)(\bar{b}\bar{\nu}_\ell)$ is very similar to that from $pp \to \tilde{b}_1^* \tilde{b}_1 \to (b\tilde{\chi}_1^0)(\bar{b}\tilde{\chi}_1^0)$ in a supersymmetric (SUSY) model, where $\tilde{b}_1$ is the lightest bottom squark and $\tilde{\chi}_1^0$ is the lightest neutralino. Therefore, we can straightforwardly adopt the way of this type of SUSY search at the LHC in this category. The ATLAS official prospects for this SUSY search at 14 TeV were communicated in Ref. [62], assuming that each $\tilde{b}_1$ decays into $b\tilde{\chi}_1^0$ with a 100% branching ratio. Details of the analysis cuts are almost the same with the 8 TeV analysis which gave the lower mass bound ~650 GeV for a massless $\tilde{\chi}_1^0$ [51]. In our analysis for the $(b\nu_\ell)(\bar{b}\bar{\nu}_\ell)$ final states, we follow the method in Refs. [51,62]. Before proceeding with the leptoquark case, we reproduce the 14 TeV prospects for the bottom squark search reported in Ref. [62] in order to verify our methodology and confirm that our result is robust.

1. Procedure of our analysis

At first, we describe the procedure of our event simulation and cut analysis. Later, we apply this procedure to the SUSY and S_1 leptoquark cases.

The final state of our targeting process is categorized as "two b jets with missing particles." Trigger cuts for reconstructed objects are required to be $p_T > 20$ GeV, $|\eta| < 2.8$ for jets; $p_T > 7$ GeV, $|\eta| < 2.47$ for electrons; and $p_T > 6$ GeV, $|\eta| < 2.4$ for muons [51], where p_T and η are transverse momentum and pseudorapidity, respectively. After that, an isolation cut based on the distance between two objects, defined as $\Delta R = \sqrt{(\Delta\eta)^2 + (\Delta\phi)^2}$, is imposed on each pair of objects. The isolation $\Delta R > 0.2$ is required between jet and light lepton candidates to remove jet candidates, and then $\Delta R > 0.4$ is required afterward
to remove light lepton candidates [51]. Finally, we also require a lepton veto.

The above step is followed by event selection cuts for our analysis. We summarize it in Table III. We require $E_T^{\rm miss} > 150$ GeV for the missing transverse energy and $p_T(j_{1(2)}) > 150(130)$ GeV for the leading (second) jet transverse momentum. The two leading jets are then required to be b-tagged. Events are discarded if any other additional jets are hard enough ($p_T > 50$ GeV). For rejecting QCD multijet backgrounds, we use the two variables $\Delta\phi_{\rm min}$ and $m_{\rm eff}(k)$ which are defined as

$$\Delta\phi_{\rm min} = \min\left(|\phi_1 - \phi_{\mathbf{p}_T^{\rm miss}}|, |\phi_2 - \phi_{\mathbf{p}_T^{\rm miss}}|, |\phi_3 - \phi_{\mathbf{p}_T^{\rm miss}}|\right), \tag{26}$$

$$m_{\rm eff}(k) = \sum_{i=1}^{k} (p_T^{\rm jet})_i + E_T^{\rm miss}. \tag{27}$$

The variable $\Delta\phi_{\rm min}$ describes the minimal azimuthal distance ($\Delta\phi$) between any of the three leading jets and the $\mathbf{p}_T^{\rm miss}$ vector. The variable $m_{\rm eff}(k)$ indicates the scalar sum of the p_T up to the kth leading jet and $E_T^{\rm miss}$. They are required to satisfy the condition $\Delta\phi_{\rm min} > 0.4$ and $E_T^{\rm miss}/m_{\rm eff}(2) > 0.25$. The invariant mass of the two b-tagged jets m_{bb} is used for suppressing backgrounds with two b jets, (from single/double top productions and Z bosons in association with heavy-flavor jets), required as $m_{bb} > 200$ GeV.

As the final step, we adopt contransverse mass cuts for the signal region A (SRA)[5] in Refs. [51,62], which is effective for the case of large mass splitting between parent and invisible-daughter particles in the decays (corresponding to $\tilde{b}_1$ and $\tilde{\chi}_1^0$ for the SUSY case, S_1 and ν for the leptoquark case). The boost-corrected contransverse mass $m_{\rm CT}$ is designed to measure the masses of pair-produced semi-invisibly decaying heavy particles [63,64] and defined as

$$m_{\rm CT}^2 = [E_T(v_1) + E_T(v_2)]^2 - [\mathbf{p}_T(v_1) - \mathbf{p}_T(v_2)]^2, \tag{28}$$

for the case of two identical decays of heavy particles (v_1 and v_2) into two visible and invisible particles. As for the choice of $m_{\rm CT}$ thresholds, the six subdivisions of SRA, such as $m_{\rm CT} > 300$, 350, 450, 550, 650, 750 GeV as in Ref. [62], are prepared in advance. Among them, an appropriate threshold is selected so that a signal significance is maximized for each model parameter point $(M_{\tilde{b}_1}, M_{\tilde{\chi}_1^0})$.

2. SUSY case

Computation method for signal event.—To reproduce the results of the 14 TeV prospects in the MSSM, we utilize the default MSSM model file provided by FeynRules [65,66] to generate signal events. Since the production process

[5]In the previous analysis [51] at 8 TeV by ATLAS, another signal region, SRB, targets scenarios with small mass splitting between the parent (bottom squark) and invisible-daughter (neutralino) particles. This is not the case for the S_1 leptoquark since the counterpart of the neutralino is the neutrino and the mass splitting is always large.

$pp \to \tilde{b}_1^* \tilde{b}_1$ is produced by QCD interactions and $\mathcal{B}(\tilde{b}_1 \to b\tilde{\chi}_1^0) = 100\%$ is assumed, relevant model parameters for the process $pp \to \tilde{b}_1 \tilde{b}_1^* \to b\bar{b}\tilde{\chi}_1^0 \tilde{\chi}_1^{0*}$ are the masses of the bottom squark $M_{\tilde{b}_1}$ and neutralino $M_{\tilde{\chi}_1^0}$. Thus, we investigate (reproduce) discovery potentials and exclusion limits on the plane of $(M_{\tilde{b}_1}, M_{\tilde{\chi}_1^0})$ at the 14 TeV LHC, setting all the other mass parameters as 10^6 GeV to be decoupled.

For parton-level event generations, we use the event generator MadGraph5_aMC@NLO version 2.2.2 [67,68] with the PDF set `CTEQ6L` [69]. At the 14 TeV LHC, jets become harder and considering jet merging becomes more important. In our setup, we examine merged events with one and two additional hard jet(s) in the k_T MLM matching scheme [70–73] with $x_q^{\rm cut} = M_{\tilde{b}_1}/4$.

The effects of parton-showering, hadronization, and jet merging are simulated by the Pythia-pgs package [74] implemented in MadGraph5_aMC@NLO, and the resultant events are recorded in the `StdHep` format. Detector simulations are performed using DelphesMA5tune [75], a modified version of Delphes 3 [76] provided in the expert mode of MadAnalysis5[77,78] version 1.1.11. In DelphesMA5tune, jets are found with the help of the package Fastjet [79,80]. We use the default configuration for jet-finding written in the modified Delphes card `delphesMA5tune_card_ATLAS_05.tcl`, obtained in Ref. [81] (for the anti-k_T algorithm [82] with ParameterR = 0.4 and JetPTMin = 20.0).

Cut analyses to obtain the acceptance times efficiency $A \times \varepsilon$ and the exclusion limit (using CL_s procedure [83]) are done by the expert mode of MadAnalysis5 [75,77,78]. The public analysis code of MadAnalysis5 for the process (top/bottom squarks search: 0 leptons + 2 b-jets) [84] at 8 TeV has been written by G. Chalons and is obtained in the Public Analysis Database [81]. Note that the public code MctLib which is available in Ref. [85] is used for calculating $m_{\rm CT}$ [63,64]. We use this code with minimal modification for the 14 TeV case by adding different choices in $m_{\rm CT}$ as shown in Table III. As for (mis)tagging rates for b jets, we used the p_T- and $|\eta|$-dependent b-tagging efficiencies considered in Ref. [62].

The production cross section $\sigma_{pp\to\tilde{b}_1\tilde{b}_1^*}$, necessary to evaluate the discovery and exclusion limits, is reported in Ref. [86] for 8 TeV and Ref. [87] for 14 TeV. The public codes Prospino2.1 [47,50] (NLO) and `NLL-fast` [88] (NLO and NLO + NLL) can also obtain the values. Those values were cross-checked using Prospino2.1.

Background event.—Expected numbers of events for SM backgrounds with a 300 fb^{-1} integrated luminosity at 14 TeV have been already simulated in Ref. [62]. The relevant processes are $t\bar{t}$, single top, Z + jets, W + jets, and others. The expected numbers, with statistic uncertainties, are shown for SRA in every region of $m_{\rm CT}$ in Table IV.

TABLE III. Summary of the event selection cuts (in SRA) after the physics object reconstruction (trigger cuts and isolation), based on Refs. [51,62].

Category	Cut condition (in SRA)
Lepton veto	No e/μ after the isolation
$E_{\rm T}^{\rm miss}$	>150 GeV
Leading jet $p_{\rm T}(j_1)$	>130 GeV
Second jet $p_{\rm T}(j_2)$	>50 GeV
Third jet $p_{\rm T}(j_3)$	Veto if >50 GeV
b-tagging	For leading two jets, $n_{b\rm jets} = 2$ ($p_{\rm T} > 20$ GeV, $\lvert\eta\rvert > 2.5$)
$\Delta\phi_{\rm min}$	>0.4
$E_{\rm T}^{\rm miss}/m_{\rm eff}(k)$	>0.25 for $k = 2$
m_{bb}	>200 GeV
$m_{\rm CT}$	>300, 350, 450, 550, 650, 750 GeV

We adopt the total uncertainties as used in the analysis of Ref. [62] and do not consider the pileup effect.

Test analysis.—Finally, we estimate the ranges of 95% C.L. exclusion, using the CL_s procedure, and of 5σ discovery in this SUSY case. The result is shown in Fig. 6 along with the ATLAS official result. One can see that the small differences of around $50 \sim 100$ GeV between our result and the ATLAS official one are found in the $(M_{\tilde{b}_1}, M_{\tilde{\chi}_1^0})$ plane. This amount of deviations would be expected from a difference between a simplified analysis and a full calculation. Thereby, we can conclude that our method in the analysis and simulations is reasonably good and reliable.

3. Leptoquark case

In the case of the S_1 leptoquark, the signal events from the process $pp \to S_1^* S_1 \to (b\nu_\ell)(\bar{b}\bar{\nu}_\ell)$ are generated by MadGraph5_aMC@NLO as well, where we have implemented the model file of the S_1 leptoquark with the help of FeynRules and UFO format [89]. We note that the relevant free parameter for the production process $pp \to S_1 S_1^*$ is only the S_1 mass M_{S_1}. Exclusion and discovery limits as a function of the branching ratio $\mathcal{B}(S_1^* \to b\bar{\nu}_\ell)$ and M_{S_1} are subsequently derived. Then, we follow the same steps with the SUSY case for the parton-showering, hadronization, jet merging, and detector simulations, through Pythia-pgs and DelphesMA5tune. In the leptoquark case, we adopt the PDF `NN23LO1` [90] in parton-level event generations. As for the cut analysis, we apply the same procedure as in Table III to the signal events for the S_1 leptoquark, that is, an appropriate SRA region is automatically imposed by MadAnalysis5. The LQ pair production cross section is evaluated by Prospino2.1 [47,50] at NLO, (which has also been computed in Ref. [91]). We employ the SM background events and their total uncertainties as provided in Ref. [62] for the present case. The pileup effect is not considered.

TABLE IV. Expected numbers of events for SM backgrounds with statistical errors for an integrated luminosity of 300 fb^{-1} at 14 TeV from Table 11 of Ref. [62]. The SRA regions are selected as $m_{CT} > 300, 350, 450, 550, 650, 750$ GeV.

BG type	SRA300	SRA350	SRA450	SRA550	SRA650	SRA750
$t\bar{t}$	32.6 ± 3.0	14.8 ± 2.0	4.3 ± 1.1	1.5 ± 0.7	0.6 ± 0.4	0.29 ± 0.29
Single top	146 ± 12	83 ± 8	41 ± 6	25 ± 5	12.7 ± 3.2	8.9 ± 2.5
Z + jets	508 ± 8	249 ± 5	70.5 ± 2.7	23.1 ± 1.5	9.1 ± 1.0	4.1 ± 0.7
W + jets	92 ± 5	44 ± 4	9.3 ± 1.7	2.9 ± 0.9	1.6 ± 0.8	0.9 ± 0.6
Others	5.4 ± 0.5	3.3 ± 0.4	1.59 ± 0.28	0.50 ± 0.16	0.18 ± 0.09	0.15 ± 0.08

B. $S_1^* \to c\tau$

To confirm that the S_1 leptoquark boson is the origin of the anomaly in $\overline{B} \to D^{(*)}\tau\overline{\nu}$, we should observe the nonzeroness of the couplings g_{1L}^{3i} and g_{1R}^{23*} ($i = 1$, 2, or 3). As shown in the previous subsection, we can probe the contribution of $g_{1L}^{3i} \neq 0$ through the S_1 search in the $(b\nu_\ell)(\overline{b}\overline{\nu}_\ell)$ final state. On the other hand, we need to investigate the decay $S_1^* \to c\tau$ for $g_{1R}^{23*} \neq 0$, which is not simple due to jets originating from the charm-quark (c jets) and decays of the tau lepton. A general feature of $S_1^* \to c\tau$ at the LHC is, however, similar to that of $S_1^* \to b\tau$. The process $pp \to S_1^* S_1 \to (b\tau)(\overline{b}\,\overline{\tau})$ has been analyzed by the CMS group based on the 8 TeV data in Ref. [56] and was applied to obtain the current bound by recasting the $(b\tau)(\overline{b}\,\overline{\tau})$ analysis to the $(c\tau)(\overline{c}\,\overline{\tau})$ case in Sec. III C 2. For the 14 TeV search, we directly apply a similar method in Ref. [56] to the process $pp \to S_1^* S_1 \to (c\tau)(\overline{c}\,\overline{\tau})$.

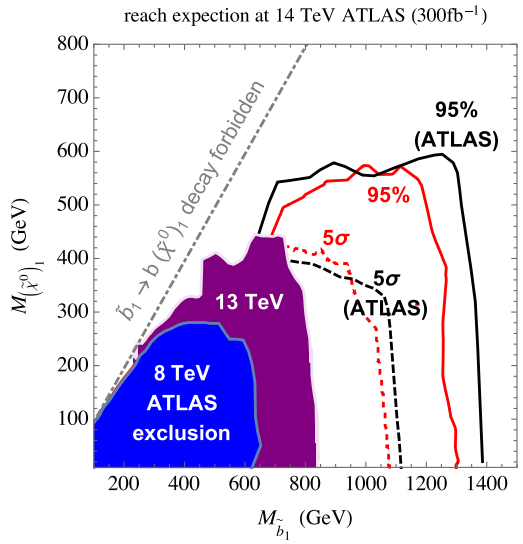

FIG. 6. The expected 95% C.L. exclusion boundary (solid lines) and the 5σ discovery reach (dashed lines) for the bottom squark pair production with 300 fb^{-1} of integrated luminosity at 14 TeV. Our evaluation and the ATLAS official report [62] are shown with red and black colors, respectively. The ATLAS detector system was adopted in our evaluation. The covered region with the blue (purple) color was already excluded by the 8 TeV (13 TeV) ATLAS analysis based on the data with 20.1 fb^{-1} (3.2 fb^{-1}) integrated luminosity [51,54].

Some optional modifications of the method (for requirements of jets and leptons) are also discussed. As for a (mis) tagging efficiency of the c jet, a further discussion is necessary and we investigate several cases as will be shown later. Our analysis method based on Ref. [56] is summarized as follows.

1. Procedure of our analysis

We focus on the events where one of the two tau leptons decays into a light lepton ℓ (electron or muon) such as $\tau \to \ell\overline{\nu}_\ell\nu_\tau$ and the other one decays hadronically (denoted as τ_h) as $\tau_h \to$ hadrons $+ \nu_\tau$. In Ref. [56], the two signal regions $e\tau_h$ and $\mu\tau_h$ are separately considered. In our analysis, we consider two cases for $\ell = \mu$ and $\ell = \mu$, e.

The trigger cuts are imposed so that the light lepton (jet) satisfies the conditions $p_T > 30$ GeV, $|\eta| < 2.1(2.4)$, and the light leptons and jets are isolated as $\Delta R > 0.5$ [56].

At the first step after the trigger cut and isolation, we require a τ_h jet. In our analysis simulation, a candidate for τ_h jet is selected among reconstructed jets by applying the conditions $p_T > 50$ GeV and $|\eta| < 2.3$. The selected candidate, along with (without) a parton-level tau lepton within the range $\Delta R < 0.5$, is classified as a true (fake) τ_h-jet candidate. Then, we identify a true (fake) candidate[6] as a real τ_h jet by taking (mis)tagging efficiency into account. For the true candidate, we uniformly use a tagging rate of 0.5, found in Refs. [92,93] in the tight operating point for the hadron plus splits (HPS) and the multivariate analysis (MVA) algorithms. The mistagging rate for the fake candidate is also obtained in Refs. [92,93] as a function of p_T. For the HPS algorithm, the following form is obtained through our data fitting:

$$(1.23193 \times 10^{-10})p_T^3 + (-1.28812 \times 10^{-7})p_T^2 + (4.81842 \times 10^{-5})p_T + (0.124279)\log p_T/p_T + (-0.00820209). \quad (29)$$

[6]For a τ_h jet originating from the true category, the electric charge of the parton-level tau lepton corresponds to that of the charge of the initial τ of τ_h. However, when a fake candidate is misidentified as a τ_h jet, the corresponding electric charge of the initial τ of τ_h is randomly determined because of the absence of the corresponding data.

In our analysis, we adopt the HPS algorithm. A major reason why we perform τ_h-jet tagging without using the function installed in DELPHESMA5TUNE is to improve statistics by accepting all events and subsequently reweighting them based on the tagging rates. The factor for reweighting is defined as the probability that only one candidate is tagged and others (if exist) are not tagged.

For the next step after τ_h-jet identification, we find c jets in a similar manner to the above. We note that in our analysis for the $(c\tau)(\bar{c}\,\bar{\tau})$ final state, we do not tag b jets since it is not necessary. Since the present detector simulation does not provide a c-jet tagging module, we need to implement it in our analysis simulation. Namely, true and fake candidates for the c jet are selected among reconstructed jets by the same condition with the τ_h-jet case. Next, we take into account (mis)tagging efficiencies of c-jet candidates. In our study, we consider three different choices for the efficiencies, reported in different studies [59,94,95]. The values are written as

$$\text{(Case 1)}\quad \epsilon_{c\to c}=50\%,\quad \epsilon_{b\to c}=20\%,\quad \epsilon_{\text{light}\to c}=0.5\%,\quad \text{from Ref. [59]}, \tag{30}$$

$$\text{(Case 2)}\quad \epsilon_{c\to c}=19\%,\quad \epsilon_{b\to c}=13\%,\quad \epsilon_{\text{light}\to c}=0.5\%,\quad \text{from Ref. [94]}, \tag{31}$$

$$\text{(Case 3)}\quad \epsilon_{c\to c}=40\%,\quad \epsilon_{b\to c}=25\%,\quad \epsilon_{\text{light}\to c}=10\%,\quad \text{from Ref. [95]}, \tag{32}$$

where $\epsilon_{c\to c}$ is a tagging rate and $\epsilon_{(b,\text{light})\to c}$ indicates a mistagging rate of the (b, light) jet as a c jet.

We comment on the three types of ratios. The values in Eq. (30), used in the analysis of Ref. [59], are highly desirable, where a rather high tagging probability and small mistagging ratios are assumed. The second choice in Eq. (31) was adopted in the analysis by ATLAS to search for a charm squark pair production at 8 TeV in Ref. [94], where the 95% C.L. lower bound on $M_{\tilde{c}}$ is obtained at around 560 GeV assuming a massless neutralino and $\mathcal{B}(\tilde{c}\to c\tilde{\chi}_1^0)=100\%$. Here, the c-tagging rate is quite low compared with the first category in Eq. (30), while the mistagging probabilities are still suppressed. For identifying c jets, the ATLAS group has developed the algorithm called JETFITTERCHARM [95]. The values in the third category are also provided from Ref. [95] through the JETFITTERCHARM algorithm in a different operating point, where the c-tagging rate is emphasized but the mistagging rates are also enhanced, especially from light jets. Such high mistag rates would lead to serious deterioration in background rejection. Later, we provide a quantitative comparison of the impact of these three choices in our simulation.

Another important aspect of c jets is whether at least one or at least two c jets should be required in our analysis. The former choice is better for earning statistics, while the latter one definitely has better performance in background rejection. We perform analyses following both of the criteria, the number of c jets to be at least one or two, for a better understanding of c-jet identification.

TABLE V. Summary of the event selection cuts after the physics object reconstruction, which is mainly based on the choices in [56]. Details of each cut are found in the main text.

Category	Cut and selection rule
Leptons	(A-1) one τ_h and one $\ell=\mu$ (A-2) one τ_h and one $\ell=\mu$ or e
Electric charge	Opposite sign between τ_h and $\ell^{\pm}$
Jet objects	(B-1) ≥ 3 (including τ_h) (B-2) ≥ 2 (including τ_h)
c-tagged jet	(B-1) at least two (B-2) at least one
$M(\tau_h\,\text{jet}, \text{a chosen jet})$	>250 GeV
S_T	>100–1000 GeV for each 100 GeV bin

After implementing the above procedure for the τ_h jet and c jets, we perform selections and cuts to every event. This is summarized in Table V. As mentioned above, we take account of two cases for the selection of a light lepton mode such as (A-1) $\ell=\mu$ and (A-2) $\ell=\mu$, e. We also consider the cases where the number of c jets is required to be (B-1) at least two and (B-2) at least one. The invariant mass between the τ_h jet and a chosen jet is required to be larger than 250 GeV. Which jet is used for the invariant mass is determined as follows. The two candidates $j_{1,2}$ for the jet are the leading c-tagged jet and the most leading jet among the other jets except for the already picked-up leading c jet and the τ_h jet. Finally, we adopt the selection cut as $M(\tau_h\text{-jet}, j_1)>250$ GeV when $|M(\tau_h\text{-jet}, j_1)-M(\ell, j_2)|<|M(\tau_h\text{-jet}, j_2)-M(\ell, j_1)|$ is satisfied. When the above condition failed, we chose $M(\tau_h\text{-jet}, j_2)$ for the selection cut. This procedure is based on Ref. [56] for the b-tagged jets case. The kinetic variable S_T is defined as the scalar sum of the p_T of ℓ, τ_h-jet, and the two jets $j_{1,2}$ of the two candidates for the invariant mass calculation. The selection cut of S_T is highly efficient for rejecting the irreducible $t\bar{t}$ background [56]. In our study, we prepare the cut region from 100 to 1000 GeV every 100 GeV step in advance and then choose an appropriate region to maximize the signal significance for each model parameter region.

2. Event data for signal and background

For our simulation, we generated 5×10^4 signal events for each mass of S_1 every 50 GeV bin from 350 to 1600 GeV, produced by MADGRAPH5_AMC@NLO via the process $pp\to S_1^* S_1\to(c\tau)(\bar{c}\,\bar{\tau})$ accompanying up to two additional jets (to perform jet merging). As for backgrounds, 10^7 events of $t\bar{t}$ along with up to three jets and

TABLE VI. Summary of the nominal cross sections of backgrounds in the $(c\tau)(\bar{c}\,\bar{\tau})$ channel.

Channel	Cross section	Reference	PDF
$t\bar{t}$	970.5 (pb) [NNLO + NNLL]	available in [96], (generated by TOP++V2.0 [97])	NNPDF2.3 NNLO [90] (5f FFN) (Lower PDF)
$W+$jets, $W \to \ell\nu_\ell$	7978 (pb) [W^+, NNLO + NLO EW] 5662 (pb) [W^-, NNLO + NLO EW]	generated by FEWZ [98,99]	MSTW2008NNLO [100]
$Z+$jets, $Z \to 2\ell$	1207 (pb) [NNLO + NLO EW]	generated by FEWZ [99,101]	MSTW2008NNLO [100]

$5(3) \times 10^6$ events of $W \to \ell\nu_\ell$ ($Z \to \ell\bar{\ell}$) along with up to four jets were generated for each $\ell = \mu$ and e, as well. Note that the number of generated events is not equal to the numbers of reconstruct-level events used in our cut-based analysis since $\mathcal{O}(10)\%$ events are discarded through the jet-merging procedure. The $t\bar{t}$ events are dominant backgrounds since it includes two possible mistagged c jets originating from b quarks, one τ_h jet, and one τ decaying into ℓ. The $W+$jets and $Z+$jets events give rather small contributions to the backgrounds, but might not be negligible due to their huge cross sections and possible mistagged c jets and τ_h jet. The actual values of the nominal cross sections of the three background processes are summarized in Table VI. The pure QCD background is negligible since a charged lepton is required in the final state. The single top production is subleading in the original $(b\tau)$ case [56]. Then, we ignore these two types of backgrounds in our analyses.

In addition to the analysis for the process $pp \to S_1^* S_1 \to (b\nu_\ell)(\bar{b}\bar{\nu}_\ell)$, the parton-showering, hadronization, and jet merging are done via PYTHIA-PGS. Also, the detector simulations are performed by DELPHESMA5TUNE and the reconstructed event data are stored in a root file. The NN23LO1 PDF is used for parton-level event generations of signals and backgrounds.

Then, the selections of candidate c jets and the τ_h jet, the evaluations of (mis)tagging efficiencies for c jets and the τ_h jet, and the selection cuts listed in Table V are executed in MADANALYSIS5, where we prepare the analysis code for the expert mode of MADANALYSIS5.

V. NUMERICAL RESULT

The detailed procedures of our analysis simulations aimed at the two processes, $pp \to S_1^* S_1 \to (b\nu)(\bar{b}\,\bar{\nu})$ and $pp \to S_1^* S_1 \to (c\tau)(\bar{c}\,\bar{\tau})$, are presented in Sec. IV. Based on them, we obtain prospects for the S_1 leptoquark model at the 14 TeV LHC explaining the $\bar{B} \to D^{(*)}\tau\bar{\nu}$ anomaly.

A. Prospects for the $(b\nu)(\bar{b}\,\bar{\nu})$ channel

At first, we show the prospects for the $(b\nu)(\bar{b}\,\bar{\nu})$ channel at the 14 TeV LHC in Fig. 7. The two blue solid lines indicate the exclusion limits at 95% C.L., where the first one is obtained with $\mathcal{L} = 300$ fb^{-1} and the total uncertainty in the backgrounds $\sigma_{\rm bkg}$ used in Ref. [62], whereas the other is obtained with $\mathcal{L} = 3000$ fb^{-1} and $\sigma_{\rm bkg} = 15\%$, as presented in the figure. In the latter case ($\mathcal{L} = 3000$ fb^{-1}), we expect that the background will be understood better and that $\sigma_{\rm bkg} = 15\%$ is achievable. The current observed limits from the 8 TeV searches by ATLAS and CMS, as given in Sec. III C, are also represented in the figure. The rough estimate from the ATLAS 13 TeV analysis is given as well.

The result suggests that we can discard the S_1 leptoquark up to 1.3 TeV (1.5 TeV) with $\mathcal{L} = 300$ fb^{-1} ($\mathcal{L} = 3000$ fb^{-1}), if $\mathcal{B}(S_1^* \to b\nu) = 100\%$. However, the 100% branching ratio for $S_1^* \to b\nu$ is not obtainable because g_{1L}^{3i} also controls the decay branch $S_1^* \to t\ell^i$ and then the possible value of $\mathcal{B}(S_1^* \to b\nu)$ is saturated at less than 50%. Moreover, in our setup of the model, the couplings and the S_1 mass are assumed to obey the condition in Eq. (22) to explain the $\bar{B} \to D^{(*)}\tau\bar{\nu}$ anomaly. This assumption implies that g_{1R}^{23} cannot be nonzero for a fixed nonzero g_{1L}^{3i} ($i = 3$ or 1, 2) and M_{S_1}. Furthermore, g_{1R}^{23} becomes sizable for a small g_{1L}^{3i} and a large M_{S_1}. Therefore, in practice we can investigate the leptoquark through this channel up to around 1.0 TeV (1.2 TeV) when $\mathcal{L} = 300$ fb^{-1} ($\mathcal{L} = 3000$ fb^{-1}).

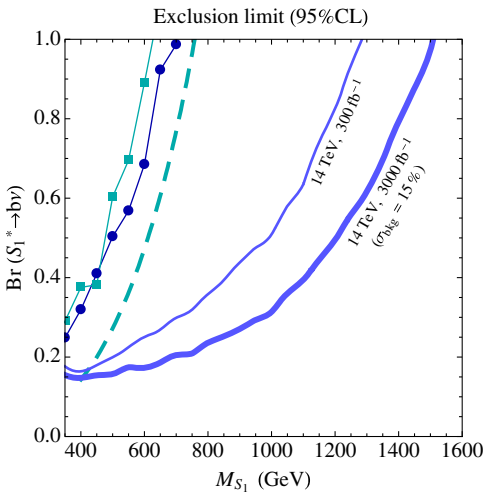

FIG. 7. Prospects for the $(b\nu)(\bar{b}\,\bar{\nu})$ channel at the 14 TeV LHC together with the constraints, given in Sec. III C, from the 8 TeV (lines with dots) and the 13 TeV (dashed line) analyses. Two kinds of expectations based on different integrated luminosities ($\mathcal{L} = 300$ fb^{-1} and $\mathcal{L} = 3000$ fb^{-1}) with background uncertainties (one from Ref. [62] and 15%, respectively) are considered as indicated in the plot.

B. Prospects for the $(c\tau)(\bar{c}\,\bar{\tau})$ channel

Next, we show the prospects for the $(c\tau)(\bar{c}\,\bar{\tau})$ channel as functions of M_{S_1} and $\mathcal{B}(S_1^* \to c\tau)$, based on the analysis method given in Sec. IV. As we explained, there are several possible selection criteria for the signal events in this channel:

(1) c-tagging and mistagging ratios: (case-1), (case-2), (case-3), as in Eqs. (30)–(32),
(2) requirement on the number of c jets: (B-1) at least two or (B-2) at least one,
(3) requirement for the light lepton flavor: (A-1) $\ell = \mu$ or (A-2) $\ell = \mu$ or e.

These points are very important since they directly affect background rejections. So, we describe their effects at length in this subsection.

In Fig. 8, we show our numerical results for the prospects in the $(c\tau)(\bar{c}\,\bar{\tau})$ channel at the 14 TeV LHC. In this figure, we consider two cases for the integrated luminosity with the background uncertainty, $\mathcal{L} = 300$ fb^{-1} with $\sigma_{\rm bkg} = 30\%$ and $\mathcal{L} = 3000$ fb^{-1} with $\sigma_{\rm bkg} = 15\%$, denoted by solid and thick solid curves, respectively. The upper panels in the figure show the results for (A-1), where the muon is required in the final state, whereas the lower panels are the results for (A-2), where the muon or electron is required. The left, middle, and right panels indicate the results obtained from the different choices of c-tagging or mistagging rates (case 1), (case 2), and (case 3), respectively, as defined in Eqs. (30)–(32). In each panel, we show two cases for the requirement on the number of c jets, (B-1) at least two and (B-2) at least one, as denoted by red and orange

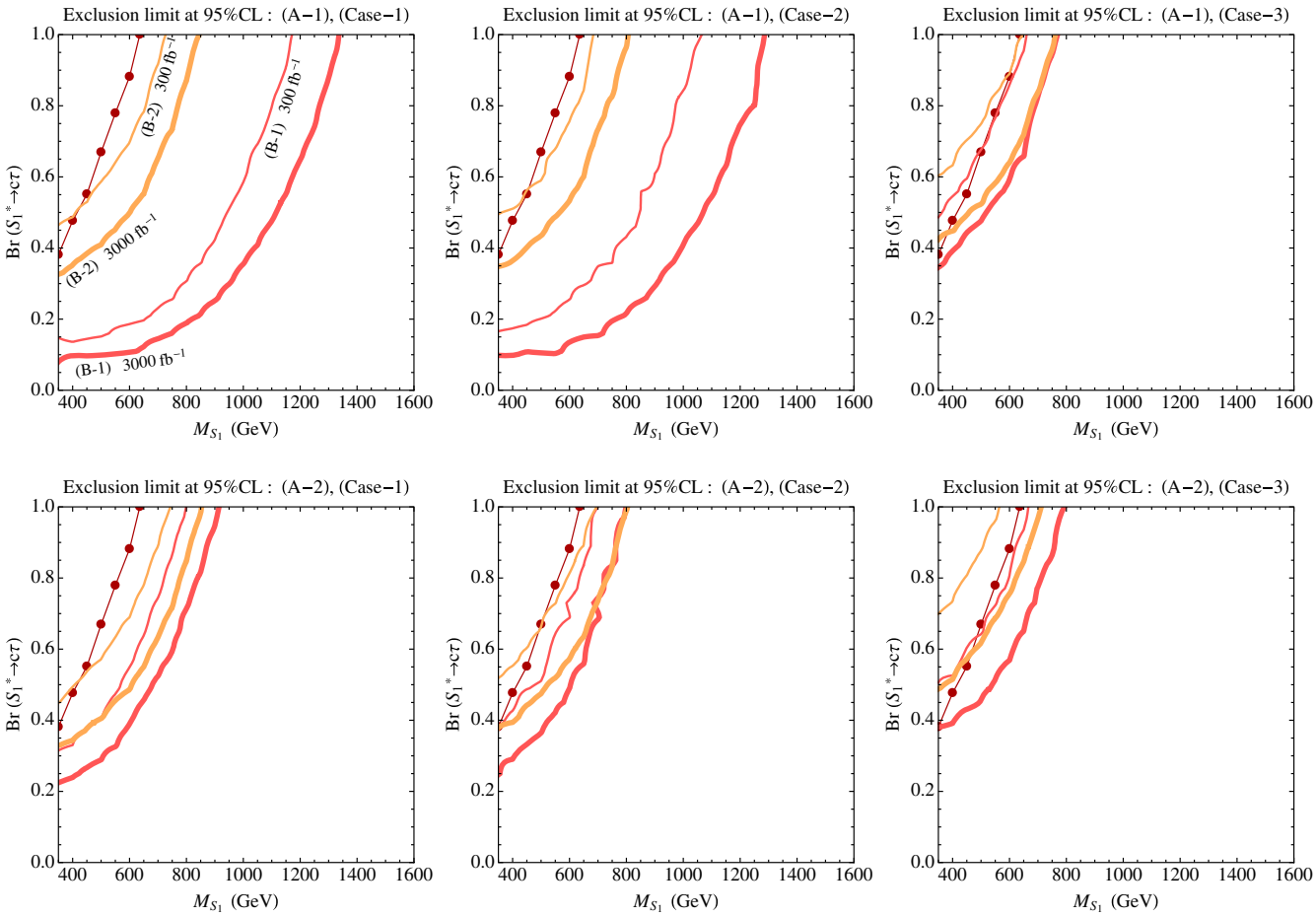

FIG. 8. Prospects for the $(c\tau)(\bar{c}\,\bar{\tau})$ channel at the 14 TeV LHC as varying (A) the requirement on the light lepton flavor, (B) the number of required c-jets, and (C) the c-tagging or mistagging rates. The solid and thick solid lines in each panel are the expected exclusion limit at 95% C.L. for the integrated luminosity with the background uncertainty, specified as $\mathcal{L} = 300$ fb^{-1} with $\sigma_{\rm bkg} = 30\%$ and $\mathcal{L} = 3000$ fb^{-1} with $\sigma_{\rm bkg} = 15\%$. The upper and lower panels show the results for (A-1) $\ell = \mu$ and (A-2) $\ell = \mu$ or e, respectively. The number of required c jets is chosen as at least (B-1) two and (B-2) one, which result in red and orange colored lines, respectively. The left, middle, and right panels indicate the result for (Case-1), (Case-2), and (Case-3), respectively, which are the three choices of c-tagging or mistagging rates adopted in our analysis. The red line with dots is the recast bound from the 8 TeV CMS analysis for $(b\tau)(\bar{b}\,\bar{\tau})$.

colors, respectively. The red line with dots in each plot indicates our recast bound from the 8 TeV CMS result on the $(b\tau)(\bar{b}\,\bar{\tau})$ channel [56]. We immediately recognize the following points:

(i) We can rank the three choices of c-tagging or mistagging rates as

$$(\text{case1}) > (\text{case2}) \gg (\text{case3}). \tag{33}$$

The result claims that (case 1) works the most effectively. This is definitely obvious since this configuration is a desired one; however such high c-tagging and low mistagging rates may be beyond the current technology. On the other hand, the efficiencies of (case 2) are already realized and used in experiment. Although the c-tagging rate in (case 2) is lower than that in (case 1), we can see that good performance is obtained in (case 2) for our model, similarly to (case 1). From the upper middle panel of Fig. 8, we conclude that we can search for the S_1 leptoquark boson through the $(c\tau)(\bar{c}\,\bar{\tau})$ channel up to 1.05 and 1.3 TeV, when accumulating $\mathcal{L} = 300\ \text{fb}^{-1}$ of data at 14 TeV with $\sigma_{\text{bkg}} = 30\%$ and $\mathcal{L} = 3000\ \text{fb}^{-1}$ with $\sigma_{\text{bkg}} = 15\%$, respectively. The last one, (case 3), is insignificant because of the high misidentification rate, especially in $\epsilon_{\text{light}\to c}$.

(ii) One can find that requiring at least two c-tagged jets, (B-1), results in the better expected exclusion than (B-2). This is simply due to the fact that the background rejection by the requirement of at least two c-jets is more efficient than that of at least one c-jet, since the c-jet tagging efficiencies are not high enough and requiring two c-jets helps us to improve separability.

(iii) The requirement for the light lepton to be muon (A-1), $\ell = \mu$, works well compared with (A-2), $\ell = \mu$ or e (note that the signal region (A-2) considers both μ and e in the same signal region). This implies that an electron channel would not significantly improve exclusion. In our analysis, we select events with one leptonic τ (and one hadronic τ). Hence, the primary background is $pp \to t\bar{t} \to b\bar{b}W^+W^-$ where one of the sequential decays is $W \to \tau\nu_\tau$. When we enlarge the allowed configuration from $\ell = \mu$ to $\ell = \mu$ or e, both of the signal and the primary background receive similar gains and the deterioration in the background overwhelms the improvement in the signal because the nominal cross section is much greater than that of the signal.

As a conclusion, the best choice in the requirements for the number of c-tagged jets and the light lepton flavor from the leptonic τ is (A-1) $\ell = \mu$ and (B-1) at least two c jets. Performances of the three types of c-tagging or mistagging rates are investigated and graded as in Eq. (33).

C. Combined results

Here, we translate the results for the expected and current exclusion limits on the branching ratios shown above into those on the coupling of the S_1 leptoquark model, in order to declare future prospects for probing the $\overline{B} \to D^{(*)}\tau\overline{\nu}$ anomaly in this model. In Fig. 9, we summarize the results for the 14 TeV LHC at 95% C.L. for $\mathcal{L} = 300\ \text{fb}^{-1}$ of accumulated data, which present prospects for the coupling

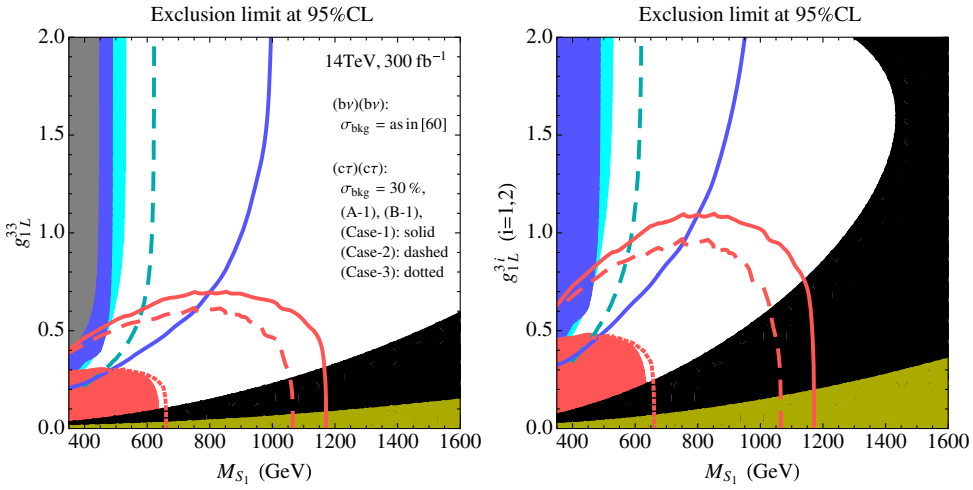

FIG. 9. Prospects for exclusions for the 14 TeV LHC when $\mathcal{L} = 300\ \text{fb}^{-1}$ data is collected. The plots present 95% C.L. exclusions for the coupling g^{3i}_{1L} and the mass M_{S_1} from both the $(b\nu)(\bar{b}\,\bar{\nu})$ and $(c\tau)(\bar{c}\,\bar{\tau})$ channels. The blue curve shows the 95% exclusion limit from the $(b\nu)(\bar{b}\,\bar{\nu})$ channel, while the red curves describe the ones from the $(c\tau)(\bar{c}\,\bar{\tau})$ channel, where the three different c-tagging or mistagging probabilities defined as (case 1), (case 2), and (case 3) are adopted in solid, dashed, and dotted curves, respectively. Here, we depict the excluded regions from the 8 and 13 TeV results. The black regions represent the areas with $\Gamma_{S_1}/M_{S_1} \geq 20\%$. The dark-yellow parts are theoretically unacceptable since $g^{23}_{1R} \geq 4\pi$.

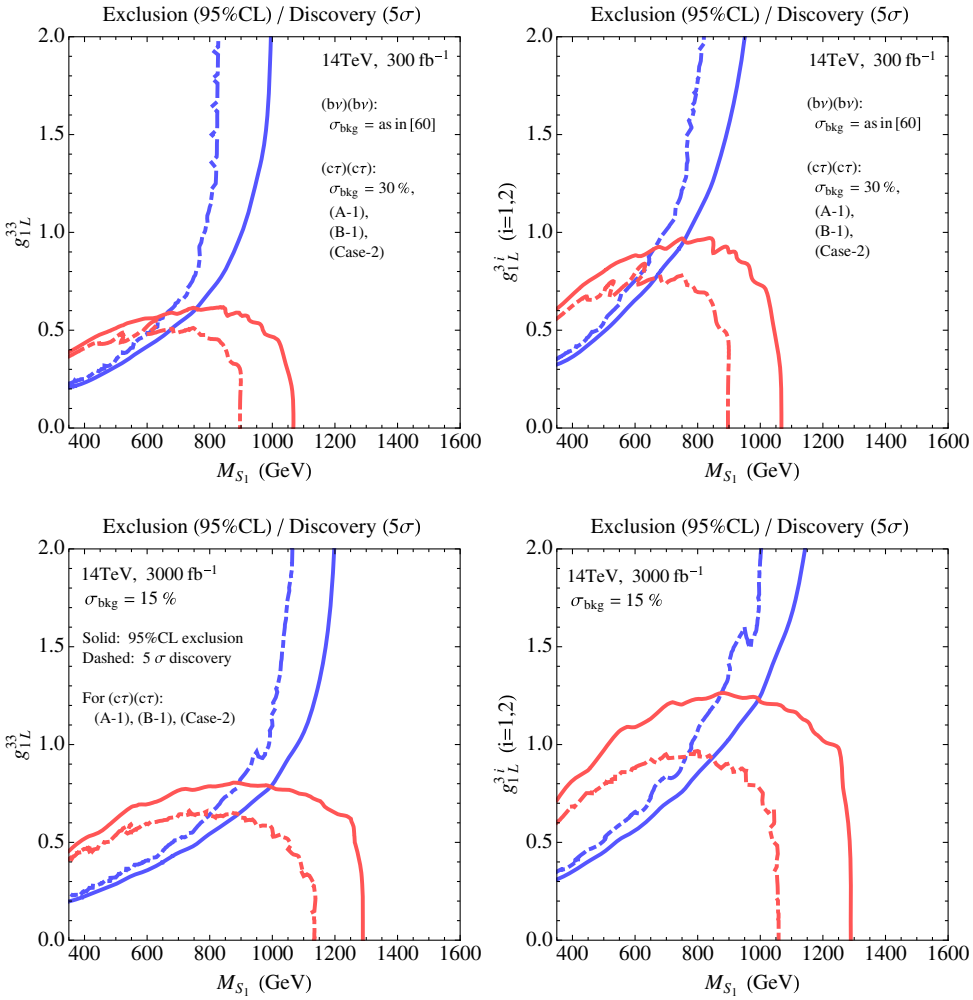

FIG. 10. Future prospects at the 14 TeV LHC with $\mathcal{L} = 300$ and 3000 fb^{-1} for 95% exclusion and 5σ discovery potentials of the S_1 leptoquark boson on the plane of (M_{S_1}, g^{3i}_{1L}). The background uncertainty is taken as $\sigma_{\rm bkg} = 30\%$ and 15%, respectively. The solid and dot-dashed curves correspond to the 95% exclusion and 5σ discovery reaches, respectively. The blue and red colors indicate the results from the $(b\nu)(\bar{b}\,\bar{\nu})$ and $(c\tau)(\bar{c}\,\bar{\tau})$ channels, respectively. For the $(c\tau)(\bar{c}\,\bar{\tau})$ case, the (A-1), (B-1), and (case 2) choices are adopted in the analysis.

g^{3i}_{1L} and the mass M_{S_1} from both the $(b\nu)(\overline{b}\,\overline{\nu})$ and $(c\tau)(\overline{c}\,\overline{\tau})$ channels. The blue curve shows the 95% exclusion limit from the $(b\nu)(\overline{b}\,\overline{\nu})$ channel, while the red curves describe the ones from the $(c\tau)(\overline{c}\,\overline{\tau})$ channel with three different c-tagging or mistagging probabilities, (cases 1, 2, 3) as defined in Eqs. (30)–(32) with solid, dashed, dotted curves, respectively. For the $(c\tau)(\overline{c}\,\overline{\tau})$ analysis, (A-1) $\ell = \mu$, (B-1) at least two c jets, and $\sigma_{\rm bkg} = 30\%$ are required in this figure. The background uncertainty for the $(b\nu)(\overline{b}\,\overline{\nu})$ channel is given as in Ref. [62] (∼30% in high $m_{\rm CT}$ signal regions), the same as before in this paper. We also show the constraints from the 8 and 13 TeV LHC data which we discussed before. The black regions represent the areas with $\Gamma_{S_1}/M_{S_1} \geq 20\%$, where the narrow-width approximation is not reliable. The dark-yellow parts should be discarded as theoretically unacceptable since perturbativity is violated for $g^{23}_{1R} \geq 4\pi$.

Note that, in our setup, the couplings $(g^{3i}_{1L}, g^{23}_{1R})$ and the mass (M_{S_1}) are related by the condition in Eq. (22) to explain the $\overline{B} \to D^{(*)}\tau\overline{\nu}$ anomaly. Hence, g^{23}_{1R} is determined with the condition in the figure. From Eq. (22), we recognize that the resultant g^{23}_{1R} tends to be larger in the case of $i = 1$ or 2 than in $i = 3$ when we compare the two cases with the common M_{S_1} and values of g^{33}_{1L} and g^{3i}_{1L} $(i = 1$ or 2) being identical. Then, the following relations are expected,

$$\mathcal{B}(S_1^* \to b\nu)|_{i=3} > \mathcal{B}(S_1^* \to b\nu)|_{i=1 \text{ or } 2},$$
$$\mathcal{B}(S_1^* \to c\tau)|_{i=3} < \mathcal{B}(S_1^* \to c\tau)|_{i=1 \text{ or } 2}. \quad (34)$$

Thus, the coverage of the 95% exclusion contour from the $(c\tau)(\overline{c}\,\overline{\tau})$ channel tends to be broader in $i = 1$ or 2 compared with $i = 3$, while the opposite trend is found

in the contour from the $(b\nu)(\bar{b}\bar{\nu})$ channel. The efficiencies of the three c-tagging or mistagging rates in cases 1, 2, 3 are directly reflected in the explored ranges as following the order in Eq. (33). Through the cooperation of the $(b\nu)(\bar{b}\bar{\nu})$ and $(c\tau)(\bar{c}\bar{\tau})$ searches with an accumulated luminosity of $\mathcal{L} = 300$ fb^{-1} at the 14 TeV LHC run II, we can exclude the S_1 leptoquark boson explaining the B physics anomaly up to at least 0.8 TeV for both $i = 3$ and $i = 1$ or 2. For small and large g_{1L}^{3i}, $M_{S_1} \lesssim 1$ TeV can be ruled out.

In Fig. 10, 95% C.L. exclusion and 5σ discovery potentials for $\mathcal{L} = 300$ and 3000 fb^{-1} at 14 TeV are shown, where the total uncertainty in the backgrounds is assumed to be $\sigma_{\rm bkg} = 30$ and 15%, and the $(c\tau)(\bar{c}\bar{\tau})$ analysis is done with (A-1), (B-1), and (case 2) choices. The 95% C.L. excluded ranges in the (M_{S_1}, g_{1L}^{3i}) parameter plane for $\mathcal{L} = 3000$ fb^{-1} are broadened as 1.0–1.3 TeV, compared with those for $\mathcal{L} = 300$ fb^{-1}. We also find that the S_1 leptoquark boson, which can explain the $\bar{B} \to D^{(*)}\tau\bar{\nu}$ anomaly, can be discovered from both the $(b\nu)(\bar{b}\bar{\nu})$ and $(c\tau)(\bar{c}\bar{\tau})$ channels with $M_{S_1} \lesssim 600/800$ GeV when we accumulate data with $\mathcal{L} = 300/3000$ fb^{-1}. There is also a possibility that the S_1 boson with $M_{S_1} \lesssim 1.1$ TeV is discovered only in either the $(c\tau)(\bar{c}\bar{\tau})$ or $(b\nu)(\bar{b}\bar{\nu})$ search.

As we have discussed, properties of jets originating from b and c quarks are similar and misidentification rates between them tend to be high in general. Due to that, it can happen that processes from the S_1 pair production other than $(b\nu)(\bar{b}\bar{\nu})$ and $(c\tau)(\bar{c}\bar{\tau})$ are detected as "signals" through our cut analysis. We call it as a misidentified signal. For example, the decay branches $S_1^* S_1 \to (t\tau)(\bar{t}\bar{\tau})$ and $S_1^* S_1 \to (c\tau)(\bar{t}\bar{\tau}), (t\tau)(\bar{c}\bar{\tau})$ fake $S_1^* S_1 \to (c\tau)(\bar{c}\bar{\tau})$ when one or two b jets via the top decay are misidentified as c-jets. Indeed, we have seen that these two misidentified signals do not change our conclusion in this paper, but are not completely negligible. We have checked that other misidentified signals are completely negligible. We explore this issue in detail in Appendix B.

VI. SUMMARY

We have investigated the LHC potential to probe the S_1 leptoquark model that can explain the $\bar{B} \to D^{(*)}\tau\bar{\nu}$ anomaly in light of existing LHC results at 8 and 13 TeV, and provided expected exclusion bounds and discovery reach at the 14 TeV LHC in terms of the parameters of this model.

At first, we have briefly reviewed the $\bar{B} \to D^{(*)}\tau\bar{\nu}$ anomaly, expressed in terms of the deviations of the observables $R(D)$ and $R(D^*)$ between the current combined experimental results and the SM predictions. It turns out that current results exhibit a deviation with significance of around 4σ. The previous studies in Refs. [10,16,30,31] suggest that the deviations can be explained by several leptoquark models. Based on Ref. [10], we have provided the latest allowed ranges for the couplings in the leptoquark models. Then we have seen that three types of leptoquark bosons, S_1, R_2, and U_1 can explain the anomaly while being consistent with all other flavor constraints.

Among them, we have focused on the S_1 leptoquark boson in order to study the LHC potential to probe the $\bar{B} \to D^{(*)}\tau\bar{\nu}$ anomaly. In order to explain the anomaly, the minimal setup yields $g_{1L}^{3i} \neq 0$, $g_{1R}^{23} \neq 0$, and vanishing values for all other couplings. The coupling g_{1L}^{3i} controls the decays $S_1^* \to t\ell^i$ and $S_1^* \to b\nu_{\ell^i}$, whereas $g_{1R}^{23} \neq 0$ gives rise to $S_1^* \to c\tau$. Since the leptoquark boson is dominantly pair produced at the LHC through QCD interactions, there are six possible channels for the signal.

Several existing 8 TeV LHC searches can be used to constrain our model. We have translated the results of ATLAS and CMS searches for pair-produced bottom squarks [51,52] decaying as $\tilde{b}_1 \to b\tilde{\chi}_1^0$ into constraints for the S_1 boson. A direct bound on the scalar leptoquark boson from $(b\nu)(\bar{b}\bar{\nu})$ was also provided by ATLAS [53]. Moreover, we have considered the constraints from the CMS search [55] for third-generation scalar leptoquark bosons decaying into $(t\tau)(\bar{t}\bar{\tau})$. We have estimated the current bound on $(c\tau)(\bar{c}\bar{\tau})$ by recasting the leptoquark search for the $(b\tau)(\bar{b}\bar{\tau})$ channel in Ref. [56]. This recasting is based on our study for the tagging and mistagging efficiencies between b and c quarks, with the help of Refs. [60,61]. Finally, preliminary results of the search for bottom squarks at the 13 TeV LHC were also taken into account. In summary, the constraints from the current available LHC searches at 8 TeV imply that $M_{S_1} < 400$ GeV, $M_{S_1} < 530$ GeV, and $M_{S_1} < 640$ GeV are ruled out for $g_{1L}^{33} \sim 0.3$, $g_{1L}^{33} \gtrsim 0.5$ and $g_{1L}^{33} \lesssim 0.2$, respectively. We reach a similar conclusion in the case of nonzero g_{1L}^{3i} $(i = 1, 2)$.

To extract a maximum potential at the 14 TeV LHC to search for the S_1 boson in our setup, we have performed detailed cut analyses that include simulation of detector effects. We have applied the cut analysis given for the $(b\tilde{\chi}_1^0)(\bar{b}\tilde{\chi}_1^{0*})$ channel to our $(b\nu)(\bar{b}\bar{\nu})$ channel and validated the expected exclusion/discovery limits on $(M_{\tilde{b}_1}, M_{\tilde{\chi}_1^0})$ in the SUSY model, as was already reported by the ATLAS Collaboration [62].

As for the cut analysis in the $(c\tau)(\bar{c}\bar{\tau})$ channel, we have employed the method for $(b\tau)(\bar{b}\bar{\tau})$ given by CMS [56] and tuned it to the 14 TeV LHC study for the $(c\tau)(\bar{c}\bar{\tau})$ signal. The following three important topics were discussed: (A) the requirement for the light lepton flavor, (B) the requirement on the number of c-jets, and (C) the c-tagging rates. In the given method, one of the tau-leptons is identified by the light lepton ℓ through the decay. In our analysis, we have considered the two cases as (A-1) $\ell = \mu$ and (A-2) $\ell = \mu$ or e. The original method for $(b\tau)(\bar{b}\bar{\tau})$ suggests that only one of the quark flavors (b) is tagged in the analysis. Instead, we have considered the two cases such that (B-1) at least two c jets and (B-2) at least one c jet

are tagged in our analysis for $(c\tau)(\bar{c}\,\bar{\tau})$. Finally, we have studied the three possibilities for the c-tagging or mistagging rates such as (case 1) from Ref. [59], (case 2) from Ref. [94], and (case 3) from Ref. [95], since the efficiency of the c-tagging algorithms at 14 TeV is not yet known.

After implementing the above method, we have generated and analyzed the signal events in the processes $pp \to S_1^* S_1 \to (b\nu)(\bar{b}\,\bar{\nu})$ and $pp \to S_1^* S_1 \to (c\tau)(\bar{c}\,\bar{\tau})$ with the use of `MadGraph5_aCM@NLO`, `pythia-pgs`, `DelphesMA5tune`, and `MadAnalysis5` in the cluster system provided at CTPU-IBS. Then we have finally obtained the exclusion limits on the S_1 leptoquark boson, expected at the 14 TeV LHC when $\mathcal{L} = 300$ fb^{-1} of data is accumulated. Our results suggest that the S_1 leptoquark boson up to at least 0.8 TeV mass can be excluded at 95% C.L. for both $i = 3$ and $i = 1$ or 2 cases of g_{1L}^{3i}. For large and small g_{1L}^{3i}, $M_{S_1} \lesssim 1$ TeV can be ruled out from the $(b\nu)(\bar{b}\,\bar{\nu})$ and $(c\tau)(\bar{c}\,\bar{\tau})$ searches, respectively. We have also evaluated the 95% C.L. exclusion and 5σ discovery potentials at a future 14 TeV center-of-mass energy, assuming that $\mathcal{L} = 3000$ fb^{-1} of data is collected and the background uncertainty is improved as $\sigma_{\rm bkg} = 15\%$. The 95% C.L. excluded ranges of M_{S_1} are changed to 1.0–1.3 TeV. It has been found that the S_1 leptoquark boson with mass less than 0.8 TeV can be discovered from both the $(b\nu)(\bar{b}\,\bar{\nu})$ and $(c\tau)(\bar{c}\,\bar{\tau})$ channels. A discovery only from either the $(c\tau)(\bar{c}\,\bar{\tau})$ or $(b\nu)(\bar{b}\,\bar{\nu})$ search can be expected up to $M_{S_1} \lesssim 1.1$ TeV. We emphasize that the $\bar{B} \to D^{(*)}\tau\bar{\nu}$ anomaly, explained by the S_1 leptoquark boson, can be probed at the LHC search only if both the signals from $(b\nu)(\bar{b}\,\bar{\nu})$ and $(c\tau)(\bar{c}\,\bar{\tau})$ are discovered.

We briefly comment on prospects for the $(t\ell)(\bar{t}\,\bar{\ell})$ final state. Although this channel has not yet been surveyed at the LHC, it may have good prospects since there are at least two charged leptons in the final state. In Ref. [102], the 95% C.L. lower bound on the mass was evaluated as $m_{\rm LQ} \gtrsim 160$ GeV for $\mathcal{B}({\rm LQ} \to t\mu) = 1$ via the $t\bar{t}$ production cross section $\sigma_{t\bar{t}}$ measured by the D0 experiment at the Tevatron, from the final state $\ell_i^{\pm}\ell_j^{\mp} + \not{E}_{\rm T} + \geq 3$ jets using 4.3 fb^{-1} data at $\sqrt{s} = 1.96$ TeV [103]. This bound is rather weak compared with $m_{\rm LQ} \gtrsim 300$ GeV, obtained by the search for the second generation leptoquark through ${\rm LQ} \to q\mu$ based on the 1.0 fb^{-1} data assuming $\mathcal{B}({\rm LQ} \to q\mu) = 1$ [104]. On the other hand, refinement of the analysis cuts would lead to improvements in the sensitivity to the $(t\ell)(\bar{t}\,\bar{\ell})$ final state (see [105,106] for the latest LHC analyses at $\sqrt{s} = 13$ TeV for the second generation leptoquark.).

Finally, we mention that the leptoquark study in this paper is a simplified one, where only two leptoquark couplings to the second and third generation fermions are nonzero, and the $SU(2)_L$ singlet S_1 leptoquark boson is chosen for simplicity. In this model, however, nonzero proton decay amplitudes are written down with renormalizable interactions in general, even though the proton decay is problematic only in the presence of nonzero couplings to the first generation fermions. A more realistic candidate would be the doublet leptoquark R_2, where proton decay does not occur at the renormalizable level. An exhaustive study including detailed collider analyses on R_2 would be an interesting further direction.

ACKNOWLEDGMENTS

We are grateful to Wonsang Cho for providing a cluster system to generate a huge number of signal and background events. We are also thankful to Dipan Sengupta for helping us with event generation of the background processes and also giving advice for the NNLO cross section for the background processes. K. N. also thanks Shigeki Matsumoto, Satoshi Mishima, Mihoko Nojiri, Takaaki Nomura, Chan Beom Park, Kohsaku Tobioka, Tsutomu Yanagida, and Hiroshi Yokoya for fruitful discussions. We acknowledge the CTPU-IBS cluster system for executing massive computations. This work is supported in part by IBS-R018-D1 for R. W. and B. D.

APPENDIX A: EXPERIMENTAL RESULTS OF $R(D)$ AND $R(D^*)$

The present experimental results from the *BABAR* experiment [1,2] have been given by

$$R(D)_{BABAR} = 0.440 \pm 0.072,$$
$$R(D^*)_{BABAR} = 0.332 \pm 0.030, \tag{A1}$$

where their correlation is reported as $\rho_{BABAR} = -0.27$. The recent results reported from the Belle [8] and LHCb [9] collaborations are shown as

$$R(D)_{\rm Belle} = 0.375 \pm 0.069,$$
$$R(D^*)_{\rm Belle} = 0.293 \pm 0.041,$$
$$\rho_{\rm Belle} = -0.36, \tag{A2}$$

$$R(D^*)_{\rm LHCb} = 0.336 \pm 0.040. \tag{A3}$$

Then we obtained the combined results as

$$R(D)_{\rm exp} = 0.393 \pm 0.048,$$
$$R(D^*)_{\rm exp} = 0.321 \pm 0.021,$$
$$\rho_{\rm exp} = -0.31. \tag{A4}$$

With using this, we have evaluated the deviations as in Eqs. (2) and (3) and plotted the contour as in Fig. 1.

We now briefly explain the way in which the observables $R(D)$ and $R(D^*)$, defined in Eq. (1), are measured. The *BABAR* Collaboration [1] reconstructed only the purely leptonic decays of the tau lepton such as $\tau^- \to e^-\bar{\nu}_e\nu_\tau$ and $\tau^- \to \mu^-\bar{\nu}_\mu\nu_\tau$, so that the signal $(\bar{B} \to D^{(*)}\tau^-\bar{\nu}_\tau)$ and the

normalization ($\overline{B} \to D^{(*)}\ell^-\overline{\nu}_\ell$ for $\ell = e$ and μ) events can be identified using the same particles in the detector. Then signal and normalization events are extracted after several parameter fits to distributions are performed. This method can reduce various sources of uncertainty in $R(D)$ and $R(D^*)$. The recent Belle result in Ref. [8] was also improved in a similar way. The analysis for the LHCb is totally different [9] since the B mesons are produced from the proton-proton collision. The muonic tau decay mode is utilized at LHCb.

As for the normalization modes $\overline{B} \to D^{(*)}\ell^-\overline{\nu}_\ell$, the averaged decay rates for $\ell = e$ and μ are used for the theoretical predictions on $R(D^{(*)})$. These decay processes have been observed to measure $|V_{cb}|$ in Refs. [107–110]. We note that differences between the results from $\ell = e$ and μ decay modes are not seen in the determination of $|V_{cb}|$, which implies that the lepton flavor universality between $\overline{B} \to D^{(*)}e^-\overline{\nu}_e$ and $\overline{B} \to D^{(*)}\mu^-\overline{\nu}_\mu$ holds within uncertainties.

APPENDIX B: MISIDENTIFIED SIGNALS

In our main study, we focused on the $(b\nu)(\overline{b}\,\overline{\nu})$ and $(c\tau)(\overline{c}\,\overline{\tau})$ channels as signal events in the search. As introduced in Sec. V C, misidentified signals, arising from other leptoquark processes than the ones primarily considered, may arise and should be discussed. In particular, the processes $S_1^*S_1 \to (t\tau)(\overline{t}\,\overline{\tau})$ and $S_1^*S_1 \to (c\tau)(\overline{t}\,\overline{\tau}), (t\tau)(\overline{c}\,\overline{\tau})$ are dominant misidentified signals in our model. They can contribute to the signal in the search for $S_1^* \to c\tau$. We have investigated such misidentified signals and evaluated their exclusion potential in the (M_{S_1}, g_{1L}^{33}) plane of the S_1 leptoquark model.

In Fig. 11, we show the 95% exclusion limits from the signal through the misidentification of $(c\tau)(\overline{t}\,\overline{\tau}), (t\tau)(\overline{c}\,\overline{\tau})$ and $(t\tau)(\overline{t}\,\overline{\tau})$, where we set $\mathcal{L} = 300$ fb^{-1}, $\sigma_{\rm bkg} = 30\%$, (A-1), and (B-1). The black curves indicate the 95% exclusion limits from the misidentified signals of $[(c\tau)(\overline{t}\,\overline{\tau}), (t\tau)(\overline{c}\,\overline{\tau})]$ and $[(t\tau)(\overline{t}\,\overline{\tau})]$ presented in the left and right panels, respectively. The solid and dashed curves are obtained for case 1 and case 2, respectively. The blue and red curves are the results from the normal signals $(b\nu)(\overline{b}\,\overline{\nu})$ and $(c\tau)(\overline{c}\,\overline{\tau})$ (for case 1 and case 2), as shown in Sec. V.

Although the misidentification of the $(c\tau)(\overline{t}\,\overline{\tau}), (t\tau)(\overline{c}\,\overline{\tau})$, and $(t\tau)(\overline{t}\,\overline{\tau})$ channels affect the evaluation of expected exclusion limits, it turns out that our conclusion obtained from the $(b\nu)(\overline{b}\,\overline{\nu})$ and $(c\tau)(\overline{c}\,\overline{\tau})$ analyses is not improved significantly when the misidentifications are taken into account. This is because that the excluded regions from these misidentified signals are fully covered by those from the original signals. The other possible misidentified signals such as $(c\tau)(\overline{b}\,\overline{\nu})$ are vetoed in the cut analysis.

Misidentifications for the signal $(b\nu)(\overline{b}\,\overline{\nu})$ can also occur. The processes $(t\tau)(\overline{b}\,\overline{\nu}), (b\nu)(\overline{t}\,\overline{\tau}), (c\tau)(\overline{b}\,\overline{\nu}), (b\nu)(\overline{c}\,\overline{\tau})$ are candidates for the misidentified signals. We have also studied these signals and found that they are completely negligible since the exclusion potentials do not exceed 60% C.L. in all regions of the parameter space.

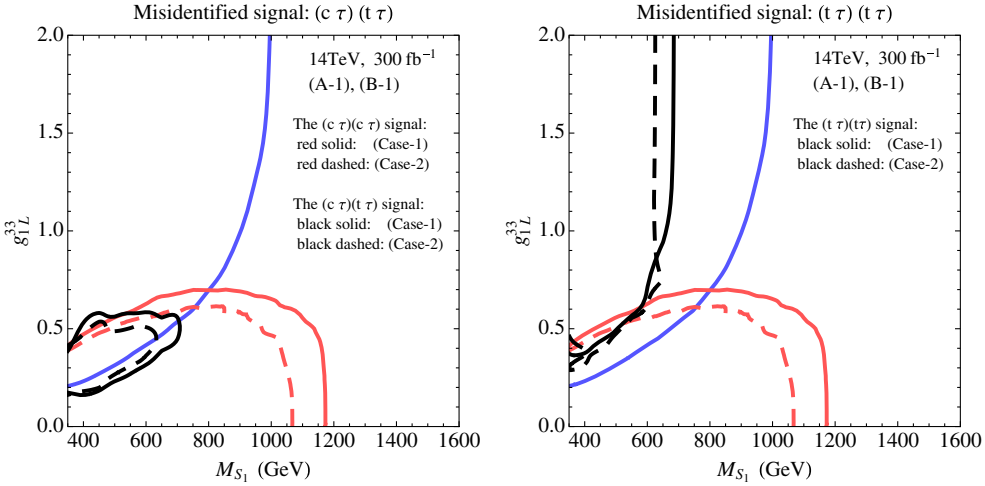

FIG. 11. The 95% exclusion limits from the misidentified signals of $S_1^*S_1 \to (t\tau)(\overline{t}\,\overline{\tau})$ and $S_1^*S_1 \to (c\tau)(\overline{t}\,\overline{\tau}), (t\tau)(\overline{c}\,\overline{\tau})$ for the 14 TeV LHC with $\mathcal{L} = 300$ fb^{-1} and $\sigma_{\rm bkg} = 30\%$, along with the results from the normal signals as given in Sec. V C. The black curves show the results of the misidentified signals, whereas the blue and red curves are from $(b\nu)(\overline{b}\,\overline{\nu})$ and $(c\tau)(\overline{c}\,\overline{\tau})$. The c-tagging or mistagging rates are chosen as indicated in the figure.

[1] J. P. Lees *et al.* (*BABAR* Collaboration), Evidence for an Excess of $\bar{B} \to D^{(*)}\tau^-\bar{\nu}_\tau$ Decays, Phys. Rev. Lett. **109**, 101802 (2012).

[2] J. P. Lees *et al.* (*BABAR* Collaboration), Measurement of an excess of $\bar{B} \to D^{(*)}\tau^-\bar{\nu}_\tau$ decays and implications for charged Higgs bosons, Phys. Rev. D **88**, 072012 (2013).

[3] A. Matyja *et al.* Belle Collaboration, Observation of $B^0 \to D^{*-}\tau^+\nu_\tau$ Decay at Belle, Phys. Rev. Lett. **99**, 191807 (2007).

[4] I. Adachi *et al.* Belle Collaboration, Measurement of $B \to D^*\tau\nu$ using full reconstruction tags, in *Proceedings, 24th International Symposium on Lepton-Photon Interactions at High Energy (LP09)*, arXiv:0910.4301.

[5] A. Bozek *et al.* Belle Collaboration, Observation of $B^+ \to \overline{D}^{*0}\tau^+\nu_\tau$ and evidence for $B^+ \to \overline{D}^0\tau^+\nu_\tau$ at Belle, Phys. Rev. D **82**, 072005 (2010).

[6] I. Caprini, L. Lellouch, and M. Neubert, Dispersive bounds on the shape of anti-B to D(*) lepton anti-neutrino form-factors, Nucl. Phys. **B530**, 153 (1998).

[7] Y. Amhis *et al.* Heavy Flavor Averaging Group Collaboration, Averages of B-Hadron, C-Hadron, and tau-lepton properties as of early 2012, arXiv:1207.1158.

[8] M. Huschle *et al.* Belle Collaboration, Measurement of the branching ratio of $\bar{B} \to D^{(*)}\tau^-\bar{\nu}_\tau$ relative to $\bar{B} \to D^{(*)}\ell^-\bar{\nu}_\ell$ decays with hadronic tagging at Belle, Phys. Rev. D **92**, 072014 (2015).

[9] R. Aaij *et al.* LHCb Collaboration, Measurement of the Ratio of Branching Fractions $\mathcal{B}(\bar{B}^0 \to D^{*+}\tau^-\bar{\nu}_\tau))/\mathcal{B}(\bar{B}^0 \to D^{*+}\mu^-\bar{\nu}_\mu)$, Phys. Rev. Lett. **115**, 111803 (2015); **115**, 159901(E) (2015).

[10] Y. Sakaki, M. Tanaka, A. Tayduganov, and R. Watanabe, Testing leptoquark models in $\bar{B} \to D^{(*)}\tau\bar{\nu}$, Phys. Rev. D **88**, 094012 (2013).

[11] W.-S. Hou, Enhanced charged Higgs boson effects in B^- → tau anti-neutrino, mu anti-neutrino and b → tau anti-neutrino + X, Phys. Rev. D **48**, 2342 (1993).

[12] M. Tanaka, Charged Higgs effects on exclusive semi-tauonic B decays, Z. Phys. C **67**, 321 (1995).

[13] J. F. Kamenik and F. Mescia, B → D tau nu branching ratios: Opportunity for lattice QCD and hadron colliders, Phys. Rev. D **78**, 014003 (2008).

[14] U. Nierste, S. Trine, and S. Westhoff, Charged-Higgs effects in a new B → D tau nu differential decay distribution, Phys. Rev. D **78**, 015006 (2008).

[15] M. Tanaka and R. Watanabe, Tau longitudinal polarization in B → D tau nu and its role in the search for charged Higgs boson, Phys. Rev. D **82**, 034027 (2010).

[16] M. Tanaka and R. Watanabe, New physics in the weak interaction of $\bar{B} \to D^{(*)}\tau\bar{\nu}$, Phys. Rev. D **87**, 034028 (2013).

[17] Y. Sakaki and H. Tanaka, Constraints on the charged scalar effects using the forward-backward asymmetry on $\bar{B} \to D^{(*)}\tau\bar{\nu}_\tau$, Phys. Rev. D **87**, 054002 (2013).

[18] J. A. Bailey *et al.*, Refining NewPhysics Searches in $B \to D\tau\nu$ Decay with Lattice QCD, Phys. Rev. Lett. **109**, 071802 (2012).

[19] S. Fajfer, J. F. Kamenik, I. Nisandzic, and J. Zupan, Implications of Lepton Flavor Universality Violations in B Decays, Phys. Rev. Lett. **109**, 161801 (2012).

[20] A. Celis, M. Jung, X.-Q. Li, and A. Pich, Sensitivity to charged scalars in $B \to D^{(*)}\tau\nu_\tau$ and $B \to \tau\nu_\tau$ decays, J. High Energy Phys. 01 (2013) 054.

[21] A. Crivellin, C. Greub, and A. Kokulu, Explaining $B \to D\tau\nu$, $B \to D^*\tau\nu$ and $B \to \tau\nu$ in a 2HDM of type III, Phys. Rev. D **86**, 054014 (2012).

[22] S. Bhattacharya, S. Nandi, and S. K. Patra, Optimal-observable analysis of possible new physics in $B \to D^{(*)}\tau\nu_\tau$, Phys. Rev. D **93**, 034011 (2016).

[23] P. Ko, Y. Omura, and C. Yu, B → D(∗) tau nu and B → tau nu in chiral U(1)' models with flavored multi Higgs doublets, J. High Energy Phys. 03 (2013) 151.

[24] J. Erler, J. L. Feng, and N. Polonsky, A Wide Scalar Neutrino Resonance and B Anti-B Production at LEP, Phys. Rev. Lett. **78**, 3063 (1997).

[25] M. Chemtob, Phenomenological constraints on broken R parity symmetry in supersymmetry models, Prog. Part. Nucl. Phys. **54**, 71 (2005).

[26] N. G. Deshpande and A. Menon, Hints of R-parity violation in B decays into $\tau\nu$, J. High Energy Phys. 01 (2013) 025.

[27] M. Freytsis, Z. Ligeti, and J. T. Ruderman, Flavor models for $\bar{B} \to D^{(*)}\tau\bar{\nu}$, Phys. Rev. D **92**, 054018 (2015).

[28] C. Hati, G. Kumar, and N. Mahajan, $\bar{B} \to D^{(*)}\tau\bar{\nu}$ excesses in ALRSM constrained from B, D decays and $D^0 - \overline{D}^0$ mixing, J. High Energy Phys. 01 (2016) 117.

[29] W. Buchmuller, R. Ruckl, and D. Wyler, Leptoquarks in lepton-quark collisions, Phys. Lett. B **191**, 442 (1987); **448**, 320(E) (1999).

[30] P. Biancofiore, P. Colangelo, and F. De Fazio, On the anomalous enhancement observed in $B \to D^{(*)}\tau\bar{\nu}_\tau$ decays, Phys. Rev. D **87**, 074010 (2013).

[31] I. Doršner, S. Fajfer, N. Košnik, and I. Nišandšić, Minimally flavored colored scalar in $\bar{B} \to D^{(*)}\tau\bar{\nu}$ and the mass matrices constraints, J. High Energy Phys. 11 (2013) 084.

[32] B. Bhattacharya, A. Datta, D. London, and S. Shivashankara, Simultaneous explanation of the R_K and $R(D^{(*)})$ puzzles, Phys. Lett. B **742**, 370 (2015).

[33] L. Calibbi, A. Crivellin, and T. Ota, Effective Field Theory Approach to $b \to s\ell\ell^{(\prime)}$, $B \to K^{(*)}\nu\bar{\nu}$ and $B \to D^{(*)}\tau\nu$ with Third Generation Couplings, Phys. Rev. Lett. **115**, 181801 (2015).

[34] M. Bauer and M. Neubert, One Leptoquark to Rule Them All: A Minimal Explanation for $R_{D^{(*)}}$, R_K and $(g-2)_\mu$, Phys. Rev. Lett. **116**, 141802 (2016).

[35] S. Fajfer and N. Kosnik, Vector leptoquark resolution of R_K and $R_{D^{(*)}}$ puzzles, Phys. Lett. B **755**, 270 (2016).

[36] R. Barbieri, G. Isidori, A. Pattori, and F. Senia, Anomalies in B-decays and $U(2)$ flavour symmetry, Eur. Phys. J. C **76**, 67 (2016).

[37] I. Doršner, S. Fajfer, A. Greljo, J. F. Kamenik, N. Konik, and I. Nišandźic, New physics models facing lepton flavor violating Higgs decays at the percent level, J. High Energy Phys. 06 (2015) 108.

[38] K. Cheung, W.-Y. Keung, and P.-Y. Tseng, Leptoquark induced rare decay amplitudes $h \to \tau^\mp\mu^\pm$ and $\tau \to \mu\gamma$, Phys. Rev. D **93**, 015010 (2016).

[39] S. Baek and K. Nishiwaki, Leptoquark explanation of $h \to \mu\tau$ and muon $(g-2)$, Phys. Rev. D **93**, 015002 (2016).

[40] J. M. Arnold, B. Fornal, and M. B. Wise, Phenomenology of scalar leptoquarks, Phys. Rev. D **88**, 035009 (2013).
[41] J.-P. Lee, *CP* violating transverse lepton polarization in B → D(∗)l anti-nu including tensor interactions, Phys. Lett. B **526**, 61 (2002).
[42] Y. Grossman, Z. Ligeti, and E. Nardi, New limit on inclusive $B \to X_s$ anti-neutrino neutrino decay and constraints on new physics, Nucl. Phys. **B465**, 369 (1996); **B480**, 753(E) (1996).
[43] R. Barate *et al.* ALEPH Collaboration, Measurements of $\mathrm{BR}(b \to \tau^- \bar{\nu}_\tau X)$ and $\mathrm{BR}(b \to \tau^- \bar{\nu}_\tau D^{*\pm} X)$ and upper limits on $\mathrm{BR}(B^- \to \tau^- \bar{\nu}_\tau)$ and $\mathrm{BR}(b \to s\nu\bar{\nu})$, Eur. Phys. J. C **19**, 213 (2001).
[44] I. Dorsner, S. Fajfer, and A. Greljo, Cornering scalar leptoquarks at LHC, J. High Energy Phys. 10 (2014) 154.
[45] J. B. Hammett and D. A. Ross, NLO leptoquark production and decay: The narrow-width approximation and beyond, J. High Energy Phys. 07 (2015) 148.
[46] T. Mandal, S. Mitra, and S. Seth, Single productions of colored particles at the LHC: An example with scalar leptoquarks, J. High Energy Phys. 07 (2015) 028.
[47] W. Beenakker, R. Hopker, and M. Spira, PROSPINO: A Program for the production of supersymmetric particles in next-to-leading order QCD, arXiv:hep-ph/9611232.
[48] M. Kramer, T. Plehn, M. Spira, and P. M. Zerwas, Pair production of scalar leptoquarks at the CERN LHC, Phys. Rev. D **71**, 057503 (2005).
[49] http://hepdata.cedar.ac.uk/view/ins1309874.
[50] http://www.thphys.uni-heidelberg.de/~plehn/index.php?show=prospino&visible=tools.
[51] G. Aad *et al.* ATLAS Collaboration, Search for direct third-generation squark pair production in final states with missing transverse momentum and two b-jets in $\sqrt{s} =$ 8 TeV pp collisions with the ATLAS detector, J. High Energy Phys. 10 (2013) 189.
[52] V. Khachatryan *et al.* CMS Collaboration, Searches for third-generation squark production in fully hadronic final states in proton-proton collisions at $\sqrt{s} = 8$ TeV, J. High Energy Phys. 06 (2015) 116.
[53] G. Aad *et al.* ATLAS Collaboration, Searches for scalar leptoquarks in pp collisions at $\sqrt{s} = 8$ TeV with the ATLAS detector, Eur. Phys. J. C **76**, 5 (2016).
[54] Tech. Report No. ATLAS-CONF-2015-066, CERN, Geneva, Dec, 2015, https://cds.cern.ch/record/2114833.
[55] V. Khachatryan *et al.* CMS Collaboration, Search for third-generation scalar leptoquarks in the tτ channel in proton-proton collisions at $\sqrt{s} = 8$ TeV, J. High Energy Phys. 07 (2015) 042.
[56] V. Khachatryan *et al.* CMS Collaboration, Search for pair production of third-generation scalar leptoquarks and top squarks in proton-proton collisions at sqrt(s) = 8 TeV, Phys. Lett. B **739**, 229 (2014).
[57] C. Delaunay, T. Golling, G. Perez, and Y. Soreq, Enhanced Higgs boson coupling to charm pairs, Phys. Rev. D **89**, 033014 (2014).
[58] G. Perez, Y. Soreq, E. Stamou, and K. Tobioka, Constraining the charm Yukawa and Higgs-quark coupling universality, Phys. Rev. D **92**, 033016 (2015).
[59] G. Perez, Y. Soreq, E. Stamou, and K. Tobioka, Prospects for measuring the Higgs boson coupling to light quarks, Phys. Rev. D **93**, 013001 (2016).
[60] CMS Collaboration, CERN Report No. CMS-PAS-BTV-13-001, http://cds.cern.ch/record/1581306.
[61] S. Chatrchyan *et al.* CMS Collaboration, Identification of b-quark jets with the CMS experiment, J. Instrum. **8**, P04013 (2013).
[62] Tech. Report No. ATL-PHYS-PUB-2014-010, CERN, Geneva, Jul, 2014.
[63] D. R. Tovey, On measuring the masses of pair-produced semi-invisibly decaying particles at hadron colliders, J. High Energy Phys. 04 (2008) 034.
[64] G. Polesello and D. R. Tovey, Supersymmetric particle mass measurement with the boost-corrected contransverse mass, J. High Energy Phys. 03 (2010) 030.
[65] N. D. Christensen and C. Duhr, FeynRules-Feynman rules made easy, Comput. Phys. Commun. **180**, 1614 (2009).
[66] A. Alloul, N. D. Christensen, C. Degrande, C. Duhr, and B. Fuks, FeynRules 2.0—A complete toolbox for tree-level phenomenology, Comput. Phys. Commun. **185**, 2250 (2014).
[67] J. Alwall, M. Herquet, F. Maltoni, O. Mattelaer, and T. Stelzer, MadGraph 5: Going beyond, J. High Energy Phys. 06 (2011) 128.
[68] J. Alwall, R. Frederix, S. Frixione, V. Hirschi, F. Maltoni, O. Mattelaer, H. S. Shao, T. Stelzer, P. Torrielli, and M. Zaro, The automated computation of tree-level and next-to-leading order differential cross sections, and their matching to parton shower simulations, J. High Energy Phys. 07 (2014) 079.
[69] J. Pumplin, D. R. Stump, J. Huston, H. L. Lai, P. M. Nadolsky, and W. K. Tung, New generation of parton distributions with uncertainties from global QCD analysis, J. High Energy Phys. 07 (2002) 012.
[70] S. Hoeche, F. Krauss, N. Lavesson, L. Lonnblad, M. Mangano, A. Schalicke, and S. Schumann, Matching parton showers and matrix elements, in *HERA and the LHC: A Workshop on the Implications of HERA for LHC Physics: Proceedings Part A. 2006*, arXiv:hep-ph/0602031.
[71] M. L. Mangano, M. Moretti, F. Piccinini, and M. Treccani, Matching matrix elements and shower evolution for top-quark production in hadronic collisions, J. High Energy Phys. 01 (2007) 013.
[72] J. Alwall *et al.*, Comparative study of various algorithms for the merging of parton showers and matrix elements in hadronic collisions, Eur. Phys. J. C **53**, 473 (2008).
[73] J. Alwall, S. de Visscher, and F. Maltoni, QCD radiation in the production of heavy colored particles at the LHC, J. High Energy Phys. 02 (2009) 017.
[74] T. Sjostrand, S. Mrenna, and P. Z. Skands, PYTHIA 6.4 Physics and Manual, J. High Energy Phys. 05 (2006) 026.
[75] B. Dumont, B. Fuks, S. Kraml, S. Bein, G. Chalons, E. Conte, S. Kulkarni, D. Sengupta, and C. Wymant, Toward a public analysis database for LHC new physics searches using MADANALYSIS 5, Eur. Phys. J. C **75**, 56 (2015).
[76] J. de Favereau, C. Delaere, P. Demin, A. Giammanco, V. Lemaître, A. Mertens, and M. Selvaggi DELPHES 3 Collaboration, DELPHES 3, A modular framework for fast

simulation of a generic collider experiment, J. High Energy Phys. 02 (2014) 057.
[77] E. Conte, B. Fuks, and G. Serret, MadAnalysis 5, A User-Friendly Framework for Collider Phenomenology, Comput. Phys. Commun. **184**, 222 (2013).
[78] E. Conte, B. Dumont, B. Fuks, and C. Wymant, Designing and recasting LHC analyses with MadAnalysis 5, Eur. Phys. J. C **74**, 3103 (2014).
[79] M. Cacciari and G. P. Salam, Dispelling the N^3 myth for the k_t jet-finder, Phys. Lett. B **641**, 57 (2006).
[80] M. Cacciari, G. P. Salam, and G. Soyez, FastJet user manual, Eur. Phys. J. C **72**, 1896 (2012).
[81] http://madanalysis.irmp.ucl.ac.be/wiki/PublicAnalysis Database.
[82] M. Cacciari, G. P. Salam, and G. Soyez, The Anti-k(t) jet clustering algorithm, J. High Energy Phys. 04 (2008) 063.
[83] A. L. Read, Presentation of search results: The CL(s) technique, J. Phys. G **28**, 2693 (2002).
[84] G. Chalons, MadAnalysis 5 implementation of ATLAS-SUSY-2013-05, doi: 10.7484/INSPIREHEP.DATA.Z4ML.3W67.2.
[85] http://mctlib.hepforge.org/.
[86] https://twiki.cern.ch/twiki/bin/view/LHCPhysics/SUSY CrossSections8TeVstopsbottom.
[87] https://twiki.cern.ch/twiki/bin/view/LHCPhysics/SUSY CrossSections14TeVstopsbottom.
[88] http://pauli.uni-muenster.de/~akule_01/nllwiki/index.php/NLL-fast.
[89] C. Degrande, C. Duhr, B. Fuks, D. Grellscheid, O. Mattelaer, and T. Reiter, UFO—The universal FeynRules output, Comput. Phys. Commun. **183**, 1201 (2012).
[90] R. D. Ball *et al.*, Parton distributions with LHC data, Nucl. Phys. **B867**, 244 (2013).
[91] T. Mandal, S. Mitra, and S. Seth, Pair production of scalar leptoquarks at the LHC to NLO parton shower accuracy, Phys. Rev. D **93**, 035018 (2016).
[92] https://twiki.cern.ch/twiki/bin/view/CMSPublic/Physics ResultsPFT.
[93] Tau ID performance plots, https://cds.cern.ch/record/1704439.
[94] G. Aad *et al.* ATLAS Collaboration, Search for Scalar Charm Quark Pair Production in pp Collisions at $\sqrt{s} =$ 8 TeV with the ATLAS Detector, Phys. Rev. Lett. **114**, 161801 (2015).
[95] Tech. Report No. ATL-PHYS-PUB-2015-001, CERN, Geneva, Jan, 2015, http://cds.cern.ch/record/1980463.
[96] https://twiki.cern.ch/twiki/bin/view/LHCPhysics/TtbarNNLO.
[97] M. Czakon, P. Fiedler, and A. Mitov, Total Top-Quark Pair-Production Cross Section at Hadron Colliders Through $O(\frac{4}{5})$, Phys. Rev. Lett. **110**, 252004 (2013).
[98] R. Gavin, Y. Li, F. Petriello, and S. Quackenbush, W physics at the LHC with FEWZ 2.1, Comput. Phys. Commun. **184**, 209 (2013).
[99] Y. Li and F. Petriello, Combining QCD and electroweak corrections to dilepton production in FEWZ, Phys. Rev. D **86**, 094034 (2012).
[100] A. D. Martin, W. J. Stirling, R. S. Thorne, and G. Watt, Parton distributions for the LHC, Eur. Phys. J. C **63**, 189 (2009).
[101] R. Gavin, Y. Li, F. Petriello, and S. Quackenbush, FEWZ 2.0: A code for hadronic Z production at next-to-next-to-leading order, Comput. Phys. Commun. **182**, 2388 (2011).
[102] S. Davidson and P. Verdier, Leptoquarks decaying to a top quark and a charged lepton at hadron colliders, Phys. Rev. D **83**, 115016 (2011).
[103] D0 note 6038-conf (winter 2010 conferences), http://www-d0.fnal.gov/Run2Physics/WWW/results/prelim/TOP/T86/T86.pdf.
[104] V. M. Abazov *et al.* D0 Collaboration, Search for pair production of second generation scalar leptoquarks, Phys. Lett. B **671**, 224 (2009).
[105] CMS Collaboration, CERN Tech. Report No. CMS-PAS-EXO-16-007, Geneva, 2016, https://cds.cern.ch/record/2139349.
[106] M. Aaboud *et al.* ATLAS Collaboration, Search for scalar leptoquarks in pp collisions at $\sqrt{s} = 13$ TeV with the ATLAS experiment, arXiv:1605.06035.
[107] B. Aubert *et al.* *BABAR* Collaboration, Determination of the form-factors for the decay $B^0 \to D^{*-}\ell^+\nu_l$ and of the CKM matrix element $|V_{cb}|$, Phys. Rev. D **77**, 032002 (2008).
[108] B. Aubert *et al.* *BABAR* Collaboration, Measurement of—V(cb)—and the Form-Factor Slope in $\overline{B} \to Dl^-\overline{\nu}$ Decays in Events Tagged by a Fully Reconstructed B Meson, Phys. Rev. Lett. **104**, 011802 (2010).
[109] W. Dungel *et al.* Belle Collaboration, Measurement of the form factors of the decay $B^0 \to D^{*-}\ell^+\nu$ and determination of the CKM matrix element $|V_{cb}|$, Phys. Rev. D **82**, 112007 (2010).
[110] R. Glattauer *et al.* Belle Collaboration, Measurement of the decay $B \to D\ell\nu_\ell$ in fully reconstructed events and determination of the Cabibbo-Kobayashi-Maskawa matrix element $|V_{cb}|$, Phys. Rev. D **93**, 032006 (2016).